Macromolecules

ARTICLE

pubs.acs.org/Macromolecules

# Disubstituted Liquid Crystalline Polyacetylene Derivatives That Exhibit Linearly Polarized Blue and Green Emissions

Benedict A. San Jose,[†] Satoshi Matsushita,[†] Yasuyuki Moroishi,[‡] and Kazuo Akagi*[,†]

[†]Department of Polymer Chemistry, Kyoto University, Katsura, Kyoto 615-8510, Japan

[‡]Institute of Materials Science, University of Tsukuba, Tsukuba, Ibaraki 305-8573, Japan

Supporting Information

**ABSTRACT:** We synthesized disubstituted liquid crystalline polyacetylene (di-LCPA) derivatives by polymerizing acetylene derivatives consisting of LC moieties either directly or indirectly attached to the main chain through flexible alkyl spacers. The di-LCPA derivatives show either enantiotropically thermotropic LC or lyotropic LC behavior. The origin of emission of substituted PAs, with respect to their substituents and structure, was elucidated. Depending on the substituents of the side chains, the polymers exhibit blue (470−485 nm) and green (500−540 nm) photoluminescence (PL) in chloroform and in cast film. The di-LCPA derivatives were macroscopically aligned using rubbing technique, and the aligned structures of the polymers are characterized in terms of main chain and side chain type alignments through XRD measurements. The emission color and alignment direction toward an external force in the di-LCPA derivatives are crucially determined by both the linkage forms (direct or indirect attachment) between the main chain and side chains and the molecular moieties (alkyl or aromatic moiety) of the side chains. The macroscopically aligned films of the polymers exhibit linearly polarized photoluminescence (LPL) with notable dichroic ratios. We fabricate multilayer electroluminescence (EL) devices using the polymers as the emissive polymer layer that emit 480 nm light with promising EL properties. We emphasize that although substituted PA derivatives are usually nonluminescent, the di-LCPA derivatives emit intense fluorescence with notable linear dichroism, and they could be promising for optically anisotropic luminescent materials.

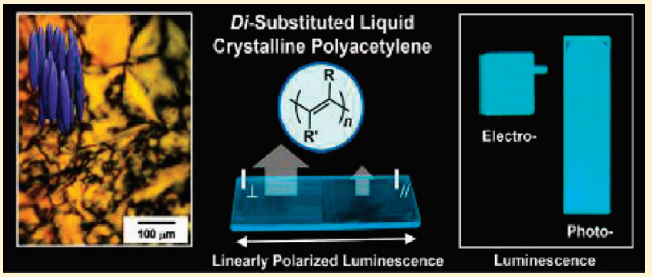


## 1. INTRODUCTION

Polymers are generally considered insulators; however, it has been demonstrated that conjugated polymers can become electrically conductive. Among these conjugated polymers, polyacetylene (PA) has attracted much attention since the discovery of its metallic conductivity in doped form. When doped with iodine, pristine PA film with a metallic luster has a black surface and a high electrical conductivity on the order of $10^4-10^5$ S/cm.[1] This discovery accelerated research on conjugated polymers and led to developments in polymeric light-emitting diodes (PLEDs),[2] plastic electronics,[3] polymer battery cells,[4] polymer photovoltaics,[5] and other novel technologies.

However, pristine PA film is insoluble in organic solvents and quickly loses its electrical conductivity when exposed to atmospheric conditions. Introducing an alkyl substituent into the polymer main chain increases solubility in organic solvents depending on the length of the alkyl chain.[6] However, the electrical conductivity of the substituted PA is significantly lower than that of the nonsubstituted PA. This phenomenon is due to less coplanarity of the main chain, which arises from steric repulsions between the substituents, a higher ionization potential, and lower electron affinity. The main chain in the substituted PA is also still randomly oriented, which suppresses the electrical conductivity of the polymer.

Adding a liquid crystalline (LC) moiety to the polymer main chain makes the polymer soluble in organic solvents and facilitates alignment by the spontaneous orientation of the LC group. For example, monosubstituted liquid crystalline PA (mono-LCPA), prepared by introducing the LC moiety into the side chain of PA, shows liquid crystallinity and stability in air.[7] It is well-known that polymers with LC moieties spontaneously align to form multidomains by virtue of the orientation of the LC moieties. Further alignment of these polymers can be achieved by applying an external force such as shear stress or an electric or magnetic field[8] to construct a monodomain structure on a macroscopic level. The schematic in Figure 1 shows the formation of multi- and monodomains through spontaneous orientation and externally forced macroscopic alignment, respectively.

Recently, we reported that mono-LCPA derivatives exhibit excellent macroscopic alignment under an applied magnetic field. Macroscopic alignment of the main chain led to both an electrical conductivity enhancement of two orders and an electrical anisotropy accompanied by the magnetically forced orientation of the LC side chain.[9]

**Received:** May 31, 2011
**Revised:** July 7, 2011
**Published:** July 29, 2011

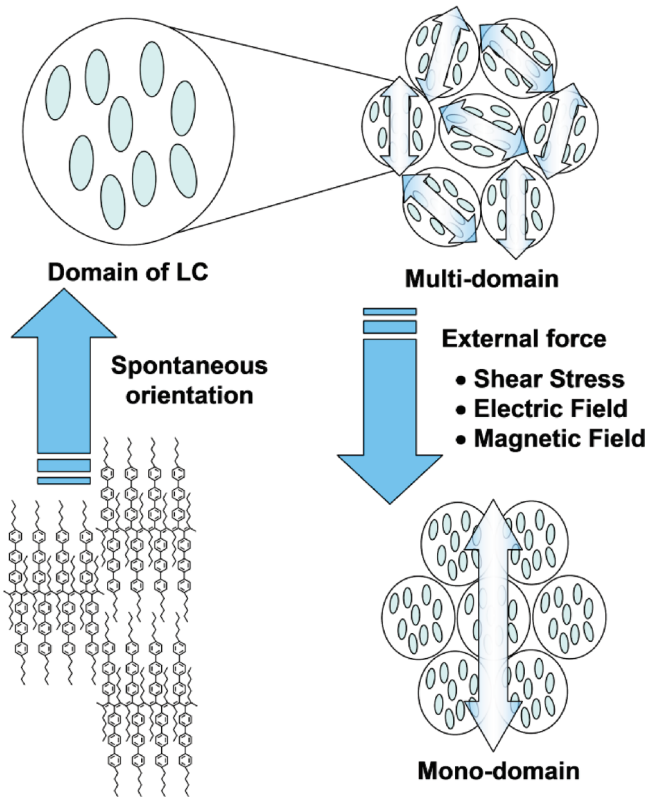


**Figure 1.** Schematic representation of the spontaneous and externally forced orientations of side chain type LC-conjugated polymers.

Aromatic conjugated polymers have outstanding electrical properties and are fluorescent. The investigation of liquid crystallinity on aromatic conjugated polymers is worthwhile. Therefore, we synthesized and studied the electrical and fluorescent anisotropies of aromatic conjugated polymers with LC side chains,[10] such as polythiophene (PT),[11] polythienylenevinylene (PTV),[11d,13] poly-*p*-phenylene (PPP),[8] poly-*p*-phenylenevinylene (PPV),[8] polypyrrole (PPy),[12] and polyaniline (PANI) derivatives.[14]

Compared to aromatic conjugated polymers such as PPP and PT, the monosubstituted PA (mono-PA) is generally considered nonemissive because of the Coulombic interactions between $\pi$-electrons.[15a] Figure 2 depicts the energy levels of ground and low-lying excited states of non-, mono-, and disubstituted polyacetylenes and the correlations between the corresponding energy states. In this figure the notations of $1A_g$, $2A_g$, and $1B_u$ are used for the intrachain excitons, and these are conserved in mono- and disubstituted polyacetylene derivatives, although their symmetries are different from nonsubstituted PA. Hence, for this series of PA derivatives, the optical transitions involving the $A_g$ and $B_u$ pair of states are symmetry-allowed, whereas those involving two $A_g$ states are symmetry-forbidden because the transition dipole moment in the direction of the main chain is strongest and its irreducible representation is $B_u$.[15e] In *trans*-PA with $C_{2h}$ symmetry (in terms of unit cell), the transition between the ground state of $1A_g$ and the excited state of $2A_g$ is electronically forbidden; however, the transition between $1A_g$ and the excited state of $1B_u$ is electronically allowed, according to the symmetry-based selection rule.[15e] For non- and monosubstituted PAs, the $1B_u$ state decays into the $2A_g$ state, but the transition from $2A_g$ to $1A_g$ is electronically forbidden. Therefore, non- and monosubstituted PAs are generally nonemissive.

When another bulky group is substituted into the mono-PA to form disubstituted PA (di-PA), the steric effect on the polyene main chain changes the relative position of the two excited states so that the $1B_u$ excited state is lower than the $2A_g$ state. This shift enables a radiative transition from the $1B_u$ state to the $1A_g$ ground state.[15] Thus, fluorescent di-PA can be synthesized by introducing a second side chain into the mono-PA main chain.

There are some reports of di-PA with PL;[17] however, there are only a few reports of macroscopic alignment in di-PA to exhibit linearly polarized luminescence (LPL).[18] The introduction of anisotropic functionality to aromatic conjugated polymers led to the development of advanced LC conjugated polymers with chiral induction,[19] ferroelectric LC (FLC),[20,22] and photoswitching.[21,22] Further development of anisotropic functionality in aliphatic conjugated polymers such as di-PA will pave the way for novel advanced functionalities. Therefore, examining LPL in di-PA is worthwhile because anisotropy in the electrical conductivity or optical properties is one of the promising functions of conjugated polymers with liquid crystallinity.

In this research, various di-PA derivatives bearing LC moieties either directly or indirectly attached using flexible alkyl spacers to the main chain were synthesized. The effects of structural variation on the functionalities of the di-PA derivatives were examined. We investigated the thermotropic and lyotropic LC of the di-PAs as well as their photoluminescent (PL) and electroluminescent (EL) properties. We aimed to generate dichroic fluorescence by combining the liquid crystallinity and fluorescent functionality of di-PA.

## 2. RESULTS AND DISCUSSION

**2.1. Synthesis and Characterization of Polymers.** Various disubstituted PA derivatives with LC moieties were synthesized, including two groups with structural variations on the alkyl side chain, mesogen core, and terminal group. Group 1 di-PAs have the LC mesogen core directly attached to the polyene main chain, and group 2 have the LC groups attached via flexible spacers (Scheme 1). Synthetic routes of the monomers and polymers are given in Scheme S1 of the Supporting Information.

**PA1** has an *n*-hexyl group and a *p*-terphenyl mesogen core linked with an *n*-pentyl moiety. **PA2** has a similar structure, but with the *p*-terphenyl mesogen linked with an *n*-octadecyloxy moiety. **PA3** has an *n*-decyl group and a *p*-biphenylcyclohexyl mesogen core linked with an *n*-pentyl moiety. **PA4** has a phenyl group and a *p*-terphenyl mesogen core linked with an *n*-pentyl moiety.

The PAs with the second group have the mesogen cores attached to the polyene main chain via flexible spacers. **PA5** has a pentylphenylcyclohexyl (PCH) group attached with an *n*-nonyloxy flexible spacer and an *n*-pentylphenyl group. **PA6** has two phenyl groups directly attached to the polyene main chain with the second phenyl having a PCH group attached via an *n*-dodecyloxy flexible spacer. **PA7** has a similar structure to **PA6**, with the phenyl group having a PCH moiety attached via a *n*-dodecyloxy flexible spacer. On the other side of the **PA7** main chain is a PCH group with an *n*-nonyloxy flexible spacer.

The monomers corresponding to the di-PA derivatives were synthesized using the Williamson reaction,[23] Sonogashira–Hagihara coupling,[24] Suzuki coupling,[25] and Mitsunobu reaction.[26] They were polymerized via a metathesis reaction using tantalum(V) pentachloride ($TaCl_5$) as a catalyst and tetra-*n*-butyltin (*n*-$Bu_4Sn$)

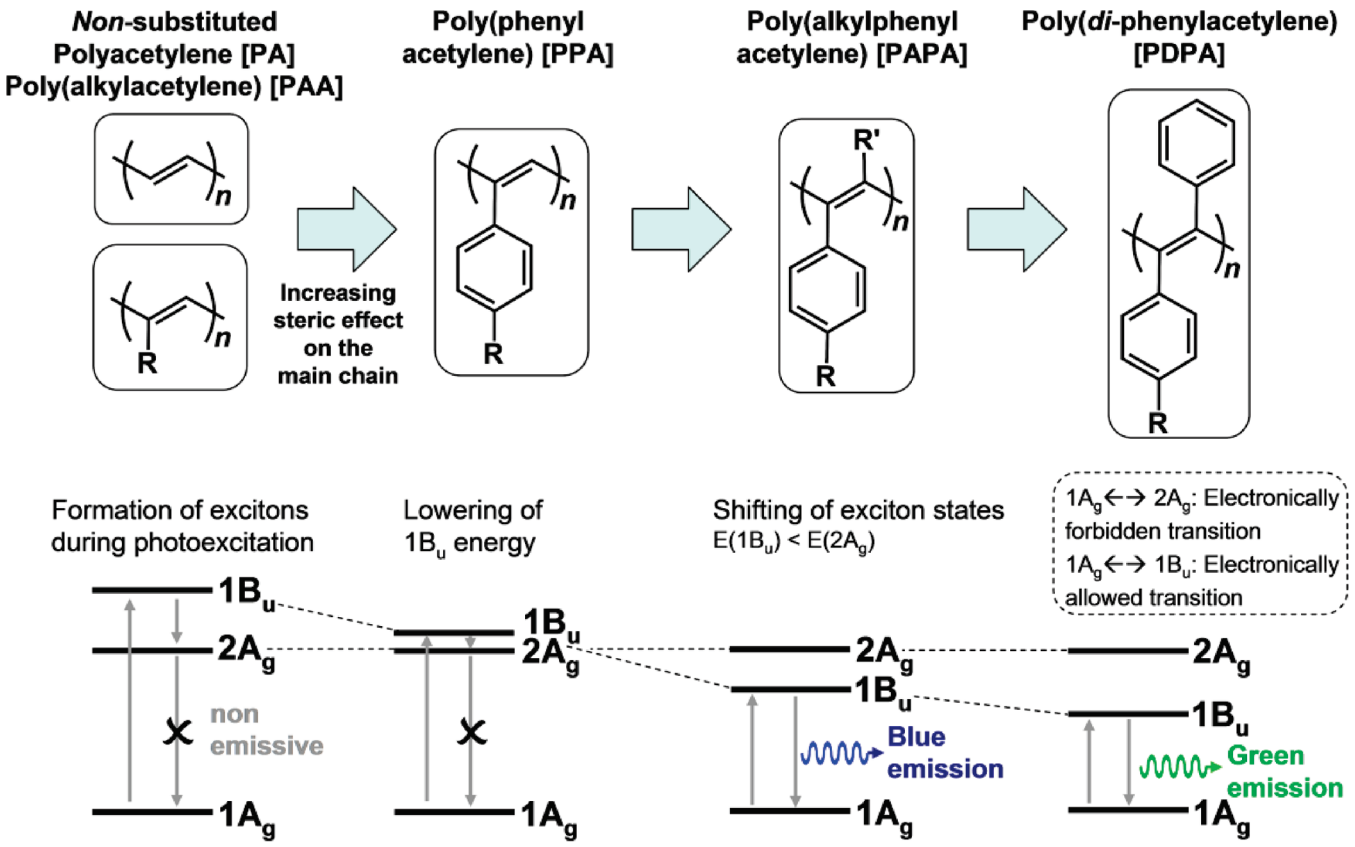


**Figure 2.** Energy levels of ground and low-lying excited states of non-, mono-, and disubstituted polyacetylenes and correlations between the corresponding energy states.

as a cocatalyst. The polymerization reaction was conducted at 80 °C under an argon atmosphere using toluene as the solvent.

The polymerization proceeded for 24 h before washing the polymer in methanol (MeOH) under constant stirring for another 24 h. The precipitated polymers were then washed in acetone for 24 h and dried under vacuum.

The number-average molecular weight ($M_n$) and the polydispersity ($M_w/M_n$) of the polymers were measured using gel permeation chromatography (GPC) and calibrated using a polystyrene (PS) standard. The GPC results showed that group 1 polymers have $M_n$ values ranging from 68 000 to 167 000 and $M_w/M_n$ values ranging from 2.4 to 3.4. The group 2 polymers had $M_n$ values ranging from 19 000 to 210 000 and $M_w/M_n$ values ranging from 1.7 to 4.5 (Table 1).

**2.2. Liquid Crystallinity.** The polymers exhibited thermal stability and thermotropic liquid crystallinity with an enantiotropic nature. LC transition temperatures of the di-PAs are shown in Figure 3.[27] Polarizing optical microscopy (POM) analysis revealed that **PA2** has a nematic LC (N-LC) phase with a Schlieren texture (Figure 4a) and no isotropic phase. The temperature ranges of the N-LC phase were 125−250 and 100−250 °C in heating and cooling processes, respectively, and thermal decomposition occurred at temperatures over 250 °C.

The LC phase of **PA2** was also investigated using X-ray diffraction (XRD). The XRD patterns reveal a single broad diffraction peak in the wide angle region (Figure 4b), typical of an N-LC phase.[28] The broad peak at 19.6° in 2$\theta$ is 4.5 Å, and it is assigned to the distance between mesogenic groups. This assignment is supported by calculations based on nonsubstituted *trans*-PA[29] whose calculated distance is ∼4.9 Å. On the basis of the present analyses, a schematic model describing the arrangement of the LC moieties within the polyene main chain is shown in Figure 4c. In this model, the *p*-terphenyl mesogens are alternately located at both sides of the polyene main chain to form a trans-transoid stereoregular configuration of head−head−tail−tail linkages.[30,31]

The two PCH mesogen cores attached via flexible spacers on **PA7** result in a smectic ($S_m$) phase (Figure 5a) with temperature ranges of 55−120 and 55−110 °C in heating and cooling processes, respectively. The XRD patterns of **PA7** have two sharp diffraction peaks at 5.2° and 19.4° in 2$\theta$ (Figure 5b), corresponding to distances of 34.4 and 4.6 Å, respectively. The former represents the smectic interlayer distance while the latter corresponds to the distance between mesogenic groups. The sharp signal in the wide angle peak of the XRD profile is typical in a hexagonal smectic B ($S_mB$) phase due to the regularity of the hexagonal packing arrangement. The 34.4 Å smectic interlayer distance ($d$) is comparable to the 36.0 Å calculated side chain length ($L_1$) of the side chain having the PCH50120P moiety,[32−35] whereas the side chain with the PCH509 moiety has a calculated side chain length ($L_2$) of 26.4 Å. The lengths of the **PA7** side chains were calculated using Spartan modeling software.

A schematic model derived from the XRD profile shows that **PA7** has a monolayer $S_mB$ phase[32−35] with hexagonal packing (Figure 5c). In this model, the PCH mesogens are attached via flexible spacers and alternate on both sides of the polyene main chain to form a trans-transoid stereoregular configuration of

**Scheme 1. Structures of the Disubstituted PA Derivatives**

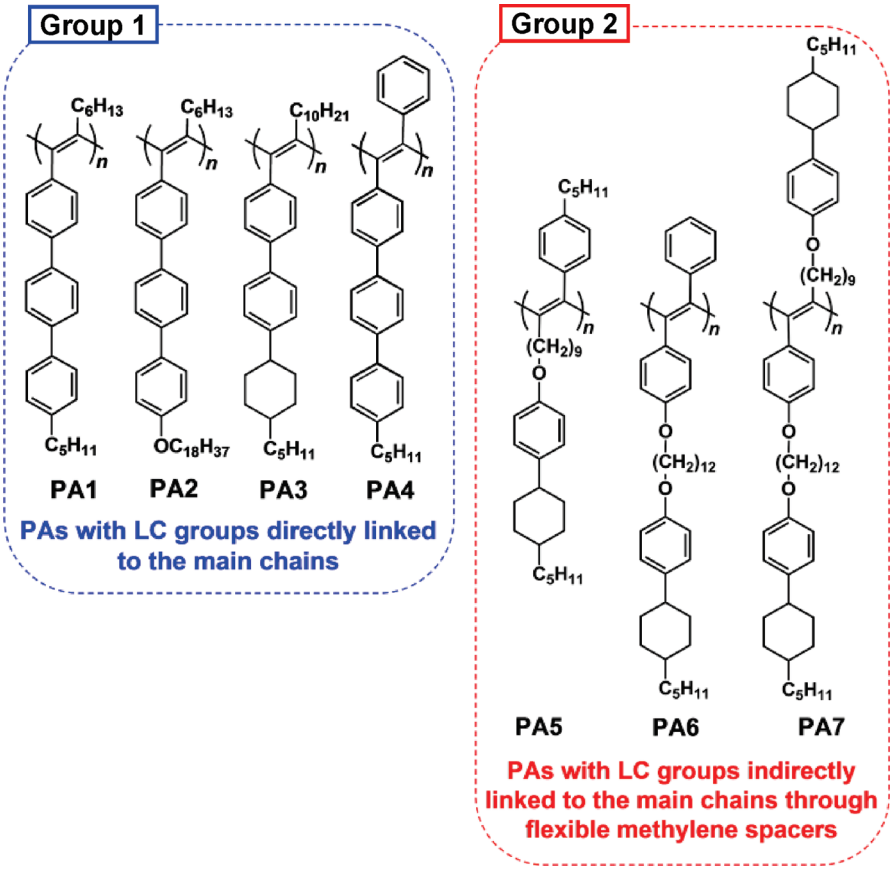


**Table 1. Results of Polymerizations of the Disubstituted PAs**

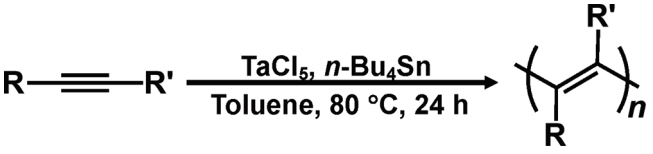


| | $M_n$ | $M_w$ | $M_w/M_n$ | DP[a] | yield (%) |
|---|---|---|---|---|---|
| **PA1** | 68 000 | 190 000 | 2.8 | 166 | 84 |
| **PA2** | 167 000 | 409 000 | 2.4 | 227 | 56 |
| **PA3** | 81 000 | 267 000 | 3.3 | 172 | 29 |
| **PA4** | 89 000 | 302 000 | 3.4 | 222 | 33 |
| **PA5** | 64 000 | 168 000 | 2.6 | 117 | 12 |
| **PA6** | 210 000 | 367 000 | 1.7 | 345 | 45 |
| **PA7** | 19 000 | 89 000 | 4.5 | 22 | 66 |

[a] Degree of polymerization.

head−head−tail−tail linkages. XRD profiles of **PA1**, **PA3**, **PA5**, and **PA6** LC films are shown in the Supporting Information, Figure S5.

Interesting trends in the LC properties are observed with changes in the structure of the PA groups. For group 1 PAs, **PA1** and **PA2** have comparable LC properties and have the same N-LC phase. The transition temperature from the glassy to the LC phase decreases from **PA1** (185 °C) to **PA3** (110 °C) during the heating process. Notably, **PA3** has an isotropic phase while **PA1** and **PA2** only degrade at high temperatures. It can also be noted that the LC temperature range in the cooling process increases from **PA1** (170−250 °C) to **PA2** (100−250 °C). Therefore, having a long alkyl chain or a bulky cyclohexyl group in the polymer structure stabilizes the LC phase. Meanwhile, **PA4** has no thermotropic LC phase. This may be due to stiffness of the polymer because it has a high degree of polymerization and the phenyl and terphenyl moieties, directly attached to the main chain, form rigid side chains based on a stilbene fragment.

Among group 2 PAs, **PA7** has a lower transition temperature (55 °C) from the glassy to LC phase than that (75 °C) of **PA5** and has an isotropic phase. This is attributed to the two PCH LC groups in the side chains of **PA7**. Conversely, **PA6** has a higher transition temperature (90 °C) from the glassy to LC phase than that of **PA5** (75 °C) because of the main chain stiffness brought about by the directly attached phenyl and phenylene groups in the side chains.

It should be emphasized here that although **PA4** has no thermotropic liquid crystallinity, it exhibits lyotropic liquid crystallinity due to its main chain stiffness enhanced by the phenyl and terphenyl moieties in side chains and relatively high molecular weight. The lyotropic LC was prepared from a 10−15 wt % solution using toluene as a solvent. Figure 6 shows the POM image of the polymer solution, depicting an optical texture characteristic of N-LC. The XRD analysis of **PA4** shows a single broad diffraction peak at 17.6° in $2\theta$. The peak corresponds to 5.0 Å, which is assigned to the distance between the mesogenic groups (see Supporting Information, Figure S1). The other


dx.doi.org/10.1021/ma201229g |*Macromolecules* 2011, 44, 6288–6302

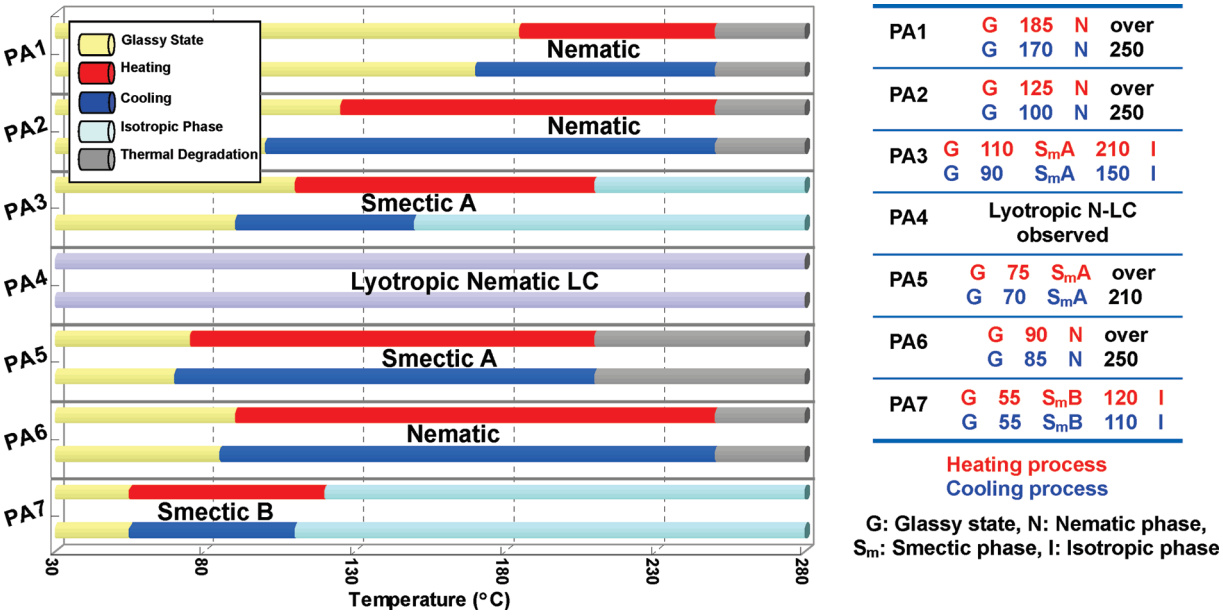


**Figure 3.** LC transition temperatures of the disubstituted PAs.

di-PAs showed no lyotropic LC phases, since the conditions necessary for achieving a lyotropic LC phase were not satisfied. Namely, to achieve a lyotropic LC phase, a stiff polymer structure with high molecular weight and a good solubility toward a solvent under an appropriate concentration at room temperature are needed.[28]

It is apparent that **PA4** has the most stiff polymer structure in terms of both of main chain and side chain among the present polymers because the side chains of **PA4** are composed of aromatic rings such as phenyl and terphenyl moieties, and these rigid moieties are directly attached to the main chain forming a stilbene fragment enforced by $\pi$-conjugation. Such a highly stiff polymer should be infusible upon the heating, resulting in no thermotropic LC. However, by virtue of pentyl group substituted at the terminal site of the terphenyl moiety, **PA4** is soluble in organic solvents such as a toluene and shows lyotropic LC. Note that the other polymers (**PA1**−**PA3**, **PA5**−**PA7**) are also soluble in organic solvents, but they show no lyotropic LC. This is probably due to their higher solubility, which might depress the formation of spontaneously aligned self-assemblies that is prerequisite to the formation of domains of lyotropic LC. In other words, the polymers with high solubility are freely dissolved in a solvent with randomly oriented conformation but form neither a regularly stacked nor an associated structure. This situation is far apart from the formation of the lyotropic LC. In the case of **PA4**, the stilbene fragment might be suitable for formation of an interchain $\pi$-electron overlapped association through van der Waals interactions, which enables the polymer to exhibit the lyotropic LC.

**2.3. Absorption and Photoluminescence.** We examined the UV−vis and PL of the di-PAs in chloroform ($CHCl_3$) solution and cast film (Table 2). Because of the *p*-terphenyl moiety, the absorption spectra of the first group of PAs in solution extend between 300 and 400 nm, corresponding to the $\pi-\pi^*$ transitions of the polyene main chains (Figure 7a). We observe an overlap between the absorption band of the polyene main chain and the *p*-terphenyl moiety at 300 nm, corresponding to the $\pi-\pi^*$ transition of the *p*-terphenyl moiety. We observe this 300 nm band in the absorption spectrum of the **PA1** monomer (Supporting Information, Figure S2). **PA5** and **PA7** have main chain absorption bands at 320 nm and a PCH mesogen absorption band at 280 nm (Figure 7b,d). Notably, **PA7** has a more defined PCH absorption peak than **PA5** due to the two PCH mesogen groups on **PA7**. Conversely, **PA6** exhibits three absorption peaks at 280, 380, and 430 nm (Figure 7c), corresponding to the absorption of the PCH moiety, the *trans*-stilbene structure, and the polyene main chain, respectively.

Figure 7 also shows the PL spectra of the PAs. The PL spectra of **PA1**, **PA2**, and **PA3** show blue colored emission, with their maximum emission ($E_{m,max}$) being around 480 nm. The **PA4** fluorescence is yellow-green with an $E_{m,max}$ at 520 nm. This difference in emission is associated with the two bulky phenyl rings directly attached to the polyene main chain which perturbs it. The perturbation lowers the $1B_u$ excited state, which decreases the band gap (Figure 2)[15] and results in a bathochromic shift of the **PA4** emission bands. The emission spectrum of **PA4** also shifts to around 540 nm in cast film, which is related to the $\pi-\pi$ stacking of the two phenyl groups directly attached to the polyene main chain in the cast film. This $\pi-\pi$ stacking increases the effective conjugation of the polyene main chain leading to the yellowish-green emission color. Polymers **PA5** and **PA7** show blue emission around 475 nm, while the two phenyl groups attached to the main chain of **PA6** cause a green luminescence at around 500 nm. There is a slight red shift to 513 nm in the PA6 cast film emission. Generally, the PAs show small emission shifts between the solution and cast film states, which is especially advantageous for applications of di-PAs as fluorescent materials in EL devices.

Fluorescence quantum yields ($\Phi$) of the PAs in solution were measured using quinine sulfate in 1.0 M sulfuric acid as the standard. The quantum yields of the PAs in solution range from 16% for **PA5** to 38% for **PA1**. This result confirms that the *p*-terphenyl moiety contributes to not only good LC properties but also effective light emission. The quantum yield values of **PA5** and **PA7** double from 16 to 30% because **PA7** has two PCH moieties which act as chromophoric pendants, leading to efficient polyene main chain emission. The emission spectrum of the


dx.doi.org/10.1021/ma201229g |*Macromolecules* 2011, 44, 6288–6302

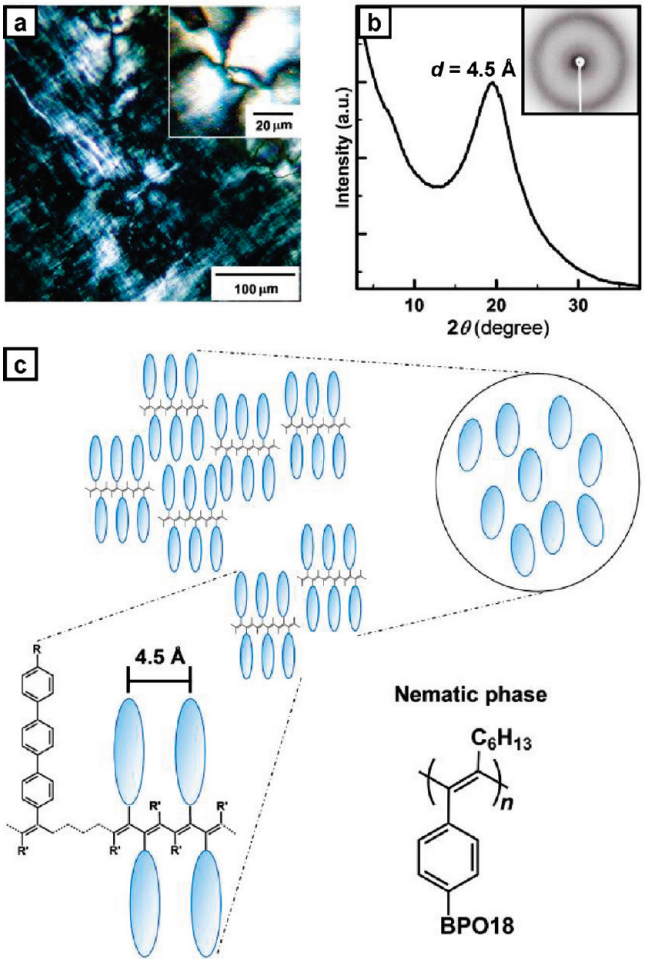


**Figure 4.** (a) POM image of **PA2** at 120 °C in cooling process. Inset shows a Schlieren texture of the nematic LC (N-LC) phase. (b) XRD pattern of **PA2** shows a broad reflection at 4.5 Å (19.6° in 2$\theta$). Inset shows the Laue pattern of **PA2**. (c) Liquid crystalline arrangement of **PA2** showing a N-LC phase.

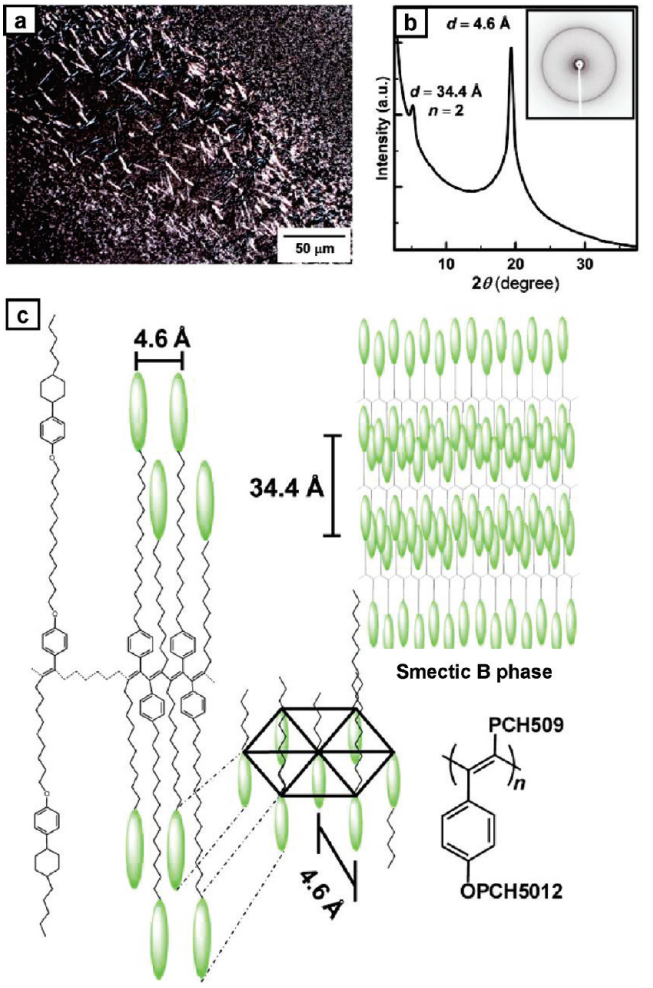


**Figure 5.** (a) POM image of **PA7** at 110 °C in cooling process. (b) XRD pattern of **PA7** shows sharp reflections at 34.4 Å (5.2° in 2$\theta$) and at 4.6 Å (19.4° in 2$\theta$). Inset shows the Laue pattern of **PA7**. (c) Liquid crystalline arrangement of **PA7** showing a hexagonal packing of the smectic B ($S_mB$) phase.

PCH pendants overlap with the polyene main chain absorption spectrum, enabling efficient emission from the PAs because of fluorescence resonance energy transfer (FRET).[17,36] Absolute fluorescence quantum yields of the PAs in cast film were also measured using integrating-sphere method with quantum yields ranging from 5% for **PA6** to 36% for **PA5**.

**2.4. Linearly Polarized Luminescence.** The macroscopic alignment of PA films was achieved using rubbing technique. Polymers on quartz substrates were heated to the LC temperature region and rubbed with a glass rod along the long axis of the quartz substrate before cooling to room temperature. In the case of **PA4**, lyotropic LC solution in 10−15 wt % toluene was prepared, then applied to a quartz substrate, and then rubbed with a glass rod along the long axis. The PL intensity was measured as a function of the polarizer angle with respect to rubbing direction. The dichroic ratio (DR) of the PAs are summarized in Table 3 and are defined as the ratio of parallel to perpendicularly polarized PL intensity (DR = $I_{\parallel}/I_{\perp}$) or vice versa (DR = $I_{\perp}/I_{\parallel}$).

Three patterns of alignment and emission behavior were observed on the aligned PA films (see Figure 9). The alignment behavior of the PA films can be related to the structure of the

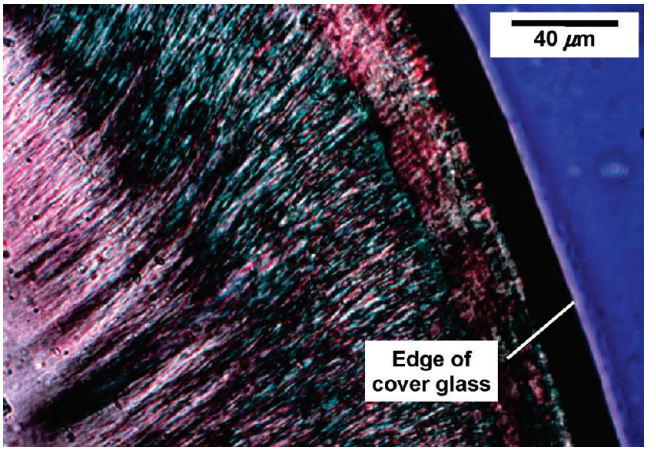


**Figure 6.** POM image of **PA4** showing a lyotropic nematic LC (N-LC) phase at room temperature. The lyotropic N-LC was prepared from 10−15 wt % solution using toluene as a solvent.

polymer main chain and the LC moieties. In the di-PA derivatives, the main chain and the side chain can both act as LC

**Table 2. Maximum Absorbance ($\lambda_{max}$), Emission ($E_{m,max}$), and Excitation ($E_{x,max}$) and Quantum Yield ($\Phi$) of the Di-PAs**

| | $\lambda_{max}$ (nm) | | $E_{m,max}$ (nm) | | $E_{x,max}$ (nm) | | $\Phi$ | |
|---|---|---|---|---|---|---|---|---|
| | in $CHCl_3$ | in film | in $CHCl_3$ | in film | in $CHCl_3$ | in film | in $CHCl_3$[a] | in film[b] |
| **PA1** | 291 | 294 | 484 | 478 | 270 | 289 | 38 | 31 |
| **PA2** | 298 | 301 | 481 | 472 | 275 | 310 | 29 | 24 |
| **PA3** | 269 | 274 | 481 | 470 | 285 | 310 | 24 | 22 |
| **PA4** | 298 | 300 | 520 | 542 | 273 | 366 | 22 | 19 |
| **PA5** | 276 | 277 | 475 | 433 | 329 | 335 | 16 | 36 |
| **PA6** | 279 | 272 | 497 | 513 | 389 | 371 | 26 | 5 |
| **PA7** | 279 | 278 | 471 | 429 | 310 | 310 | 30 | 12 |

[a] Using quinine sulfate as standard sample. [b] Using integrating-sphere method.

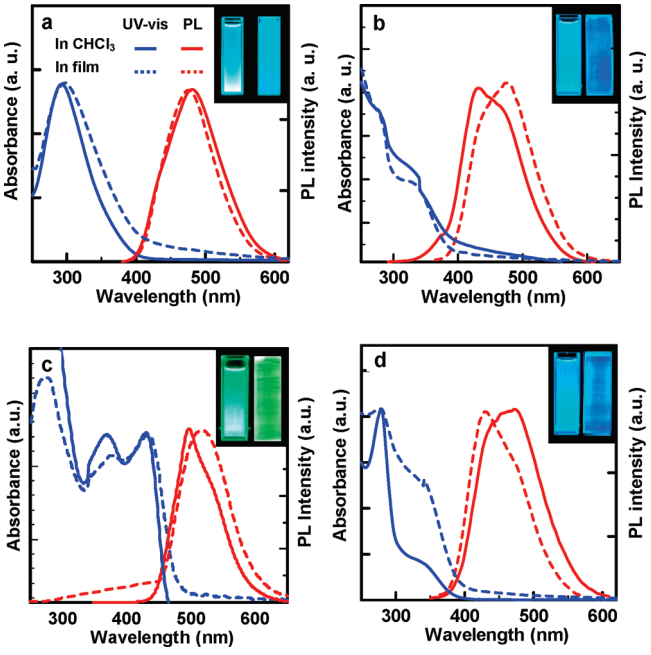


**Figure 7.** UV−vis and PL spectra of (a) **PA1**, (b) **PA5**, (c) **PA6**, and (d) **PA7** in solution and in cast film. Insets: PL in solution (left) and in cast film (right).

**Table 3. Linearly Dichroic Ratios of the Disubstituted PAs**

| | polymers[a] | dichroic ratio |
|---|---|---|
| group 1 | PA1 | 1.8 |
| | PA2 | 1.6 |
| | PA3 | 1.5 |
| | PA4 | 2.2 |
| group 2 | PA5 | 1.2 |
| | PA6 | 2.4 |
| | PA7 | 1.6 |

[a] Aligned films of **PA1**−**PA3** and **PA5**−**PA7** were prepared in thermotropic LC states, and that of **PA4** was prepared in lyotropic LC state.

mesogens. The interactions between the main chain and the LC moieties determine the alignment behavior of the PA films.

On the other hand, the emission behavior of the PA films can be related to the di-PAs exciton confinement (localization)−deconfinement (delocalization) mechanism.[15a,c,d] Excitons are electron−hole pairs that are formed during photoexcitation.[16] For the di-PAs, the excitons are initially confined (localized) to the polyene main chain because of steric effects between the bulky side chains (Figure 8a). They then are deconfined (delocalized) to the phenyl moieties where they radiatively recombine (Figure 8b). The structures of the polyene main chain and the phenyl moieties of the di-PAs determine the polymer emission behavior.

In case 1, as represented by **PA2**, we observe that **PA2** has a DR of 1.6 and a higher PL intensity perpendicular to the rubbing direction (Figure 9a). The reflection of the *p*-terphenyl moiety was observed at the meridian parallel to the rubbing direction in the XRD profile of the aligned **PA2** film (Figure 9b). These results imply that the *p*-terphenyl moiety and hence the polyene main chain are aligned perpendicular and parallel to the rubbing direction, respectively (Figure 9c). For **PA2**, the excitons are moved to the *p*-terphenylvinyl moiety through deconfinement; thus, the dominant emission of **PA2** is from the *p*-terphenylvinyl moiety with the LPL perpendicular to the rubbing direction. **PA1**, **PA2**, and **PA3** exhibit the same LPL trends where the polymers show main chain type LC alignment and dominant emission brought about by the *p*-terphenylvinyl or *p*-biphenylcyclohexylvinyl moieties directly linked to the polyene main chain.

The DR of **PA5** is 1.2, with a higher PL intensity perpendicular to the rubbing direction (Figure 9d). The XRD pattern of aligned **PA5** film shows a meridional reflection at the small angle area of 5.7° in $2\theta$ corresponding to the main chain interlayer distance of 31 Å ($n = 2$). An equatorial reflection at 18.0° in $2\theta$ was also observed (Figure 9e). This reflection can be assigned as the distance of 4.9 Å between LC moieties aligned parallel to the rubbing direction.

Given the **PA5** LPL spectra and XRD profile, we propose an alignment structure where the polyene main chain and the LC moieties are perpendicular and parallel to the rubbing direction, respectively (Figure 9f). In **PA5**, the PCH LC moiety aligns parallel to the rubbing direction, and thus it exhibits side chain type LC alignment. For **PA5**, the excitons are moved to the phenylvinyl moieties along the main chain. As a consequence, the dominant emission of **PA5** is from the phenylvinyl moieties. The case 2 polymers, **PA5** and **PA7**, show the same side chain type LC alignment and emission behavior.

In case 3, as represented by **PA6**, we observe that **PA6** has a DR of 2.4 and a higher PL intensity parallel to the rubbing direction (Figure 9g). The XRD pattern of aligned **PA6** film shows an equatorial reflection at the 17.8° in $2\theta$ ($d = 5.0$ Å) corresponding to the distance between LC moieties (Figure 9h). The LPL data and the XRD results imply that the PCH LC moieties and hence the polyene main chain are aligned parallel and perpendicular to the rubbing direction, respectively (Figure 9i). In **PA6**, the PCH LC moiety aligns parallel to the rubbing direction and thus it exhibits side chain type LC alignment. The stilbene moieties aligned parallel to the rubbing direction are the dominant emission sources; thus, **PA6** exhibits a higher PL intensity parallel to the rubbing direction. Figure 10 shows an image of the LPL of **PA6** under polarizing plates. **PA4** and **PA6** exhibit side chain type LC alignment and dominant emission from the stilbene moiety. Table 4 shows the relationship of the macroscopic alignment and emission behavior of the di-LCPAs.

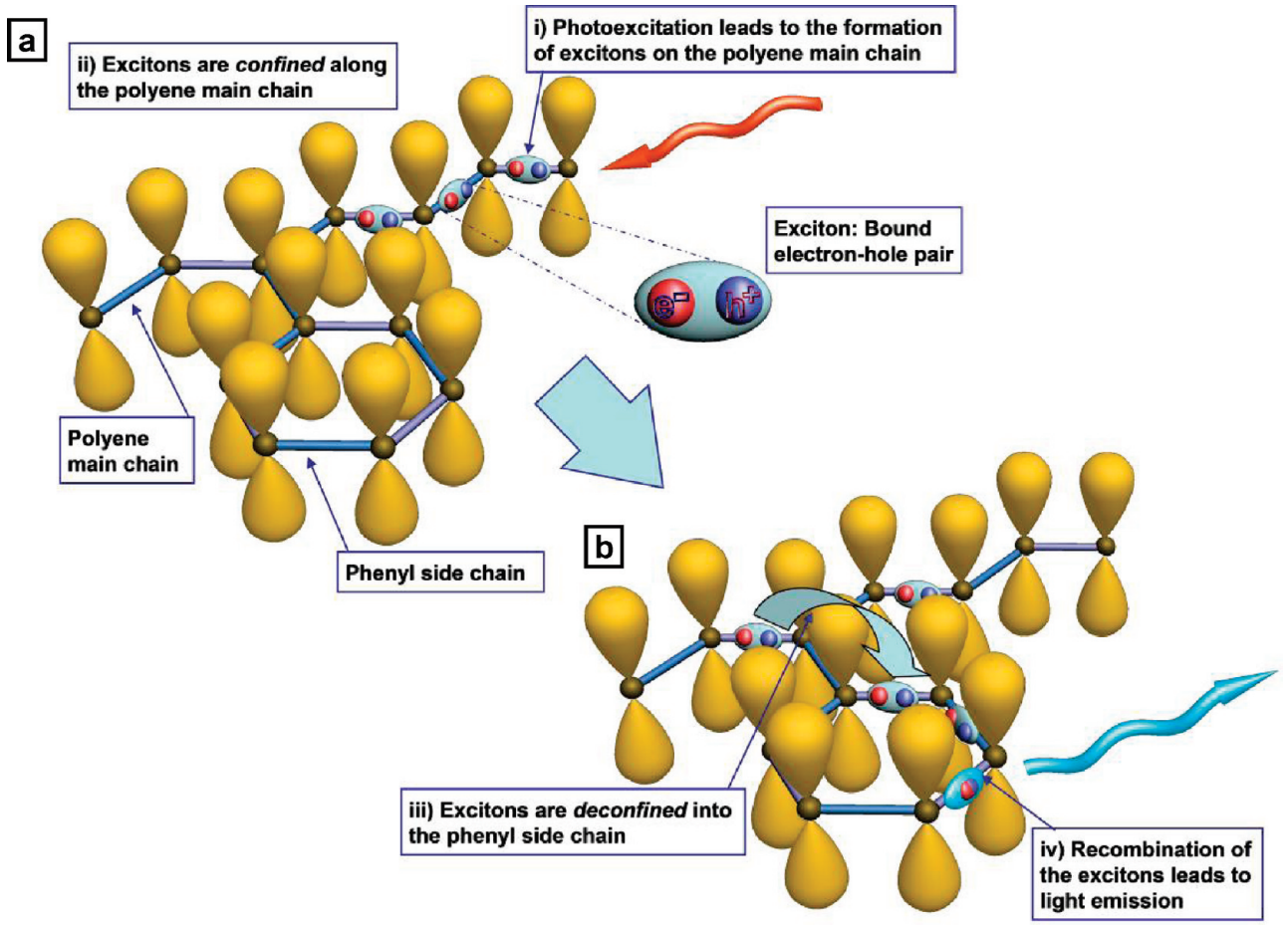


**Figure 8.** Exciton (a) confinement (localization) and (b) deconfinement (delocalization) behavior in disubstituted PA.

The PAs show LPLs with fairly low DR values that range from 1.2 to 2.4. These values are mainly due to the situation characteristic of the di-PAs where not only the LC side chain but also the conjugated polyene main chain directly linked with phenyl or phenylene moiety behave as mesogens to the external force. Since the LC side chain and the main chain are almost orthogonal in the polymer structure, the externally forced alignments of the side and main chains substantially cancel each other out, thus giving a low degree of alignment.

**2.5. Relationships between Polymer Structure, Alignment Type, and Emission Color.** At this stage, it is helpful to summarize the relationships between polymer structure, alignment type, and emission color, as depicted in Figure 11.

(i) Among the polymers of group 1, **PA1**, **PA2**, and **PA3** are classified into case 1, where the terphenyl or biphenylcyclohexyl group and the alkyl group are attached to both sides of the main chain. These polymers belong to poly(alkylphenylacetylenes) [PAPAs] (see Figure 11) and show blue emission at 481−484 nm. They exhibit unexpectedly main chain type alignment in which the main chain is aligned parallel to the rubbing direction (see also Figure 9c). It remains unclear why the polymers in case 1 show the main chain type alignment upon the rubbing treatment. Nevertheless, it should be emphasized that the conjugated polyene chains directly linked with the terphenyl or biphenyl moiety play a role of mesogenic core toward an external perturbation, which is similar to the terphenyl or biphenyl moiety itself in the side chain. In other words, the polymers in case 1 have two kinds of mesogenic cores in the main chain and side chain. The existence of two kinds of mesogenic cores, that are orthogonal to each other, causes a competitive orientation between the mesogenic cores in the main and side chains, which should weaken the alignment ability of the polymer. This may be the reason why the present polymers have unexpectedly small values in dichroic ratio such as 1.5−1.8 even after alignment (see Table 3). The direction of polymer alignment under the external perturbation should be determined by a subtle balance of the two kinds of mesogenic cores in the polymer.

(ii) **PA5** and **PA7** in group 2 are classified into case 2, where the alkylphenyl group and the alkylphenylcyclohexyl (PCH) moiety linking with the decylmethylene chain are attached to both sides of the main chain. These polymers also belong to PAPAs and show blue emissions at 471−475 nm. Although the polymers in case 1 and case 2 show blue emissions, the emission bands of the polymers in case 1 are located at longer wavelengths by about 10 nm than those in case 2. This indicates that the former polymers (**PA1**, **PA2**, and **PA3**) have longer effective conjugated lengths than the latter (**PA5** and **PA7**) because the $\pi$-conjugation between the terphenyl or biphenyl group and the vinylene moiety in case 1 is stronger than that between the phenyl group and the vinylene moiety in

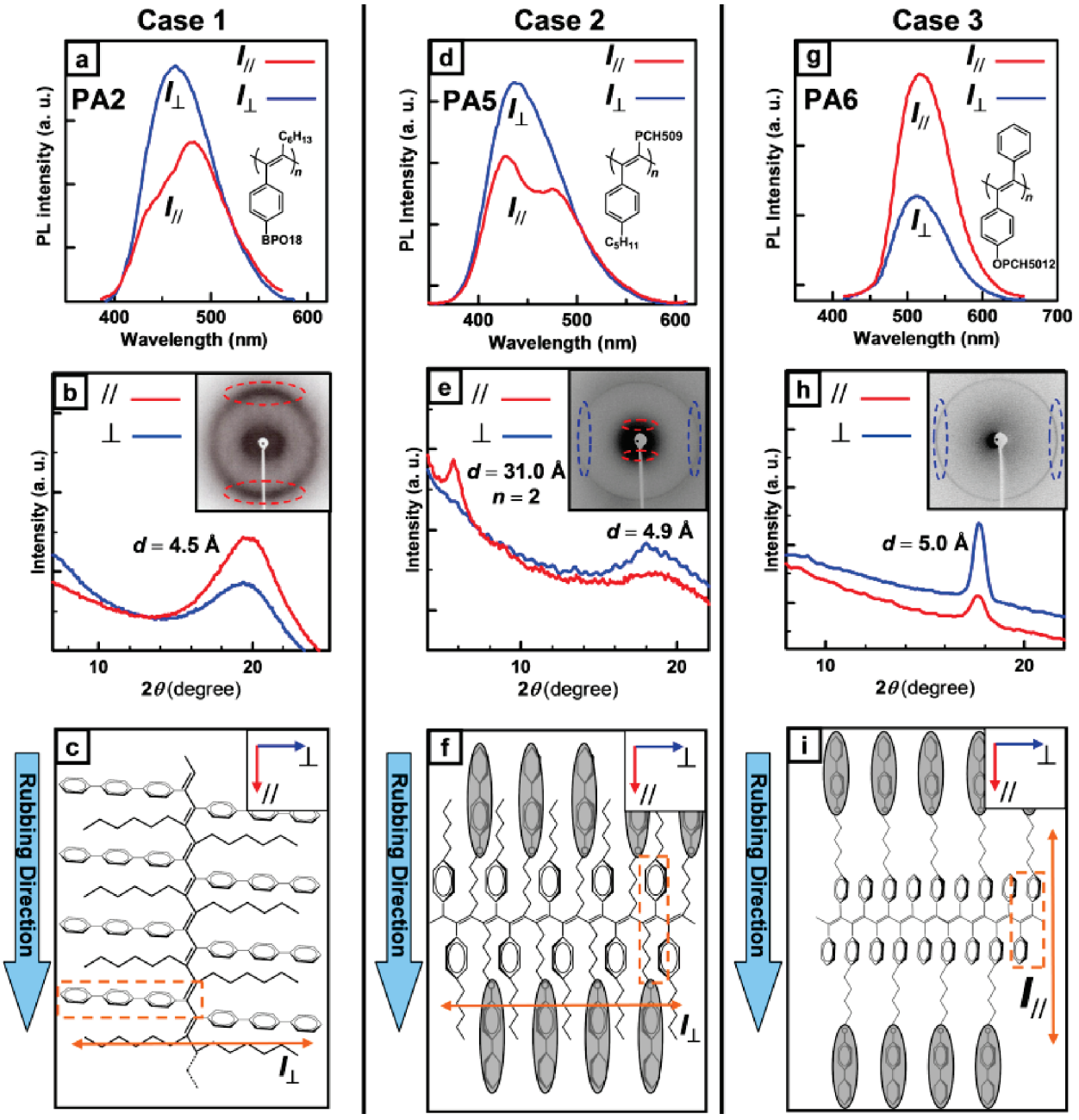


**Figure 9.** (a) Linearly dichroic PL of aligned **PA2**. (b) XRD pattern of aligned **PA2** shows a broad peak at 4.5 Å (19.6° in 2$\theta$) corresponding to the distance between the terphenyl LC moieties in the side chains. Inset: XRD Laue pattern of aligned **PA2** film. (c) Orientation diagram of aligned **PA2**. (d) Linearly dichroic PL of aligned **PA5**. (e) XRD pattern of aligned **PA5** shows peaks at 31 Å ($n$ = 2, 5.7° in 2$\theta$) and 4.9 Å (18° in 2$\theta$) corresponding to the interlayer distance of the main chains and the distance between the PCH LC moieties in the side chains, respectively. (f) Orientation diagram of aligned **PA5**. (g) Linearly dichroic PL of aligned **PA6**. (h) XRD pattern of aligned **PA6** shows a peak at 5.0 Å (17.8° in 2$\theta$) related to the distance between the PCH LC moieties in the side chains. (i) Orientation diagram of aligned **PA6**. Rectangles with orange broken lines in parts c, f, and i indicate dominant emission moieties in the polymers.

case 2. In addition, it should be noted that **PA5** and **PA7** in case 2 show side chain type alignment in which the side chain is aligned parallel to the rubbing direction (see also Figure 9f), whereas the polymers in case 1 show the main chain type alignment as mentioned above. The small dichroic ratios (1.2−1.6) in the polymers in case 2 are also rationalized with the competitive orientation occurring between the mesogenic cores of the polyene main chain and the PCH side chain (see Table 3).

(iii) **PA4** in group 1 and **PA6** in group 2 are classified into case 3, where the terphenyl or PCH-substituted phenyl group and the phenyl group are attached to both sides of the main chain, forming the poly(diphenylacetylene)s [PDPAs] (see Figure 11). The polymers show green emissions at 497−520 nm, and they show side chain type alignment. it is worth noting that the LC moiety in **PA6**, such as PCH50120P, is not directly attached to the main chain but indirectly linked to the main chain through the


dx.doi.org/10.1021/ma201229g |*Macromolecules* 2011, 44, 6288–6302

phenylene moiety. As a result, **PA6** has a stilbene type fragment consisting of a phenyl group, a vinylene moiety, and the LC-substituted phenylene moiety (see Scheme 1). Thus, **PA6** behaves as one of PDPAs in case 3 in the alignment under the external perturbation. The relatively large dichroic ratios (2.2−2.4) of the polymers in case 3 are owing to the situation that the phenyl group and the phenylene moiety or terphenyl one in the both side chains are conjugated to the vinylene moiety in the main chain to form a double mesogenic core (see Table 3 and Figure 11). This allows the side chains to align more preferably parallel to the rubbing direction, although the main chain also behaves as another mesogenic core.

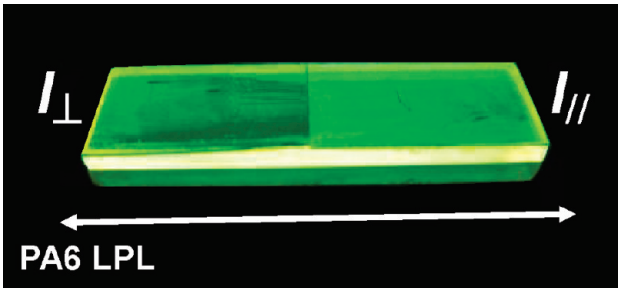


**Figure 10.** Photograph showing the LPL of **PA6**, where two polarizers are arranged parallel (bright) and perpendicular (dark) to the aligned direction. The white arrow indicates the alignment direction.

**Table 4. Different Cases of Alignment and Emission Behavior of the Disubstituted PAs**

| | polymers | alignment type | dominant emission |
|---|---|---|---|
| case 1 | **PA1**, **PA2**, **PA3** | main chain | terphenylvinyl moiety or biphenylcyclohexylvinyl moiety ($I_{\perp}$) |
| case 2 | **PA5**, **PA7** | side chain | phenylvinyl moiety ($I_{\perp}$) |
| case 3 | **PA4**, **PA6** | side chain | stilbene moiety ($I_{\parallel}$) |

As a consequence, when one designs emissive polyacetylene derivatives with linearly dichroic nature, it is essential for the polymers to have phenylene moieties that are directly or indirectly attached to the main chain and also to introduce LC moieties in one side or both side chains. However, these polymers inevitably encounter the competitive orientation or even partial cancellation in alignment between the two mesogenic cores of the rigid polyene main chain and the LC side chain that are almost orthogonal to each other. Among disubstituted PAs, the polymers bearing the double mesogenic core in side chains (**PA4** and **PA6**) are the most promising for the dichroic emissive PAs because the double mesogenic core is highly responsive to the external perturbation than the single mesogenic one, giving a alignment with substantially notable linear dichroism.

**2.6. Electroluminescence.** The PL results of the PAs led us to investigate their EL properties. We fabricated an EL device with a configuration of ITO/PEDOT−PSS (poly(3,4-ethylenedioxythiophene)−poly(styrenesulfonate))/**PA** layer/LiF/Ca/Al (Figure 12a) using **PA1** and **PA2** as the emissive polymer layer. The EL of the PAs emit at 480 nm with CIE (Commission Internationale de l'Eclairage) coordinates of (0.26, 0.33) for **PA1** and (0.21, 0.30) for **PA2**. The EL spectra of **PA1** and **PA2** show no excimer sidebands and are similar to their corresponding PL spectra. The **PA1** EL spectrum is broader and exhibits a whitish-blue-colored emission (Figure 12b). Polymers **PA1** and **PA2** have a turn-on voltage at 6−8 V and show an exponential increase in luminous intensity with values up to 220 and 50 cd/m$^2$, respectively. The EL devices utilize **PA1** and **PA2** because of their high turn-on voltage and have maximum luminous efficiencies of 0.07 and 0.08 lm/W, respectively (Table 5). Graphs showing the current efficiency, luminous efficiency, current

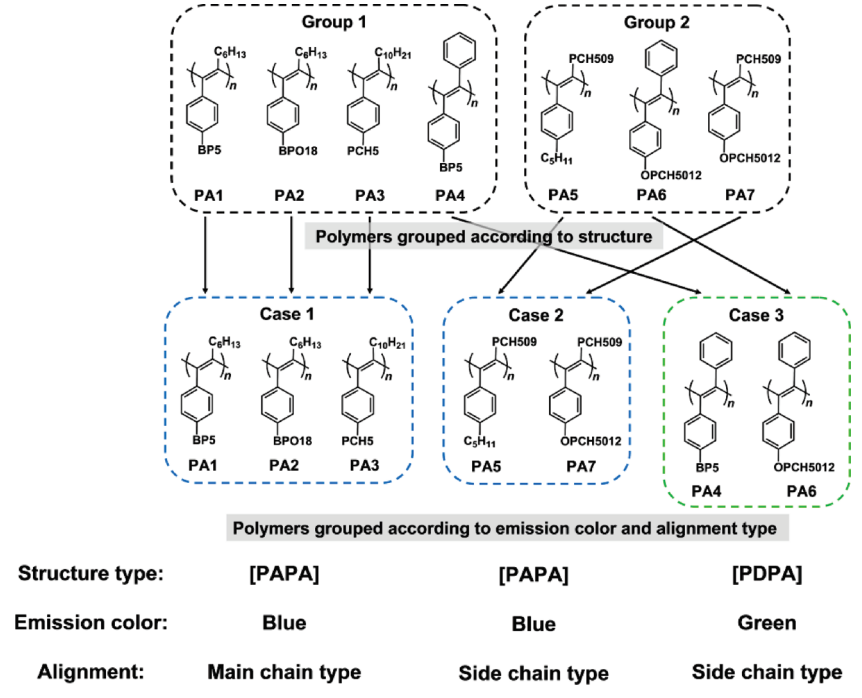


**Figure 11.** Correlation diagram summarizing the relationships between the polymer structure, emission color, and alignment type of the disubstituted PAs.


dx.doi.org/10.1021/ma201229g |*Macromolecules* 2011, 44, 6288–6302

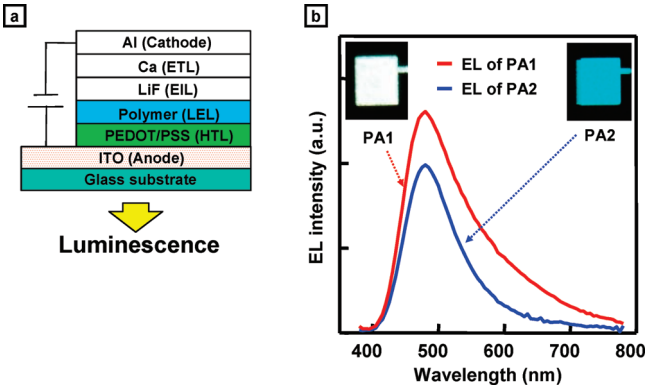


**Figure 12.** (a) Schematic diagram of the EL device using di-PA as an emissive layer. (b) EL spectra of **PA1** and **PA2**. Insets: EL spectra of **PA1** (left) and **PA2** (right).

density, and luminance of **PA1** and **PA2** are shown in the Supporting Information, Figure S6. Though EL device fabrication still needs to be optimized, we show that the use of **PA1** and **PA2** as emissive layers yield promising EL properties, suggesting that the direct attachment of the *p*-terphenyl moieties to the polyene main chain has a beneficial effect on the EL of these devices.

## 3. CONCLUSION

We synthesized disubstituted liquid crystalline PA derivatives represented by poly(alkylphenylacetylene)s [PAPAs] and poly(diphenylacetylene)s [PDPAs] and evaluated their thermal and optical properties. The polymers exhibit enantiotropically thermotropic or lyotropic liquid crystallinity. We elucidated the origin of emission of substituted PAs and also investigated fluorescent trends such as emission color and quantum yield. The polymers also show relatively low but significant PL and EL quantum yields. We found that the macroscopically aligned films of the di-PAs emit linearly polarized luminescence (LPL) by virtue of the functionalities associated with liquid crystallinity and fluorescence. The aligned structures of the di-PAs were characterized in terms of main chain and side chain type alignments through XRD measurements for the macroscopically aligned polymer films. The di-PAs were classified into three types: case 1, 2, and 3 according to the emission color and alignment type. The mechanism of LPL of the di-LCPAs with respect to the polymer structure, alignment type, and emission color was elucidated. The synthesized multifunctional disubstituted PA derivatives are thus very promising materials for applications such as advanced liquid crystal displays (LCDs) and other future applications that utilize linearly dichroic luminescent materials.

## 4. EXPERIMENTAL SECTION

**4.1. Materials.** The chemical reagents were purchased from commercially available sources and were used as received. 18-Crown-6-ether, 4-iodophenylboronic acid, and *trans*-dichlorobis(triphenylphosphine)-palladium(II) ($PdCl_2(TPP)_2$) were purchased from Aldrich Co. Ltd. Tetra-*n*-butyltin, tetrakis(triphenylphosphine)palladium(0) ($(TPP)_4Pd$), tetra-*n*-butylammonium hydroxide (TBA-OH), diethylazodicarboxylate (DEAD), 12-bromo-1-dodecanol, 1-octyne, 1-dodecyne, 4-bromo-4′-*n*-pentylbiphenyl, 4-bromo-4′-hydroxybiphenyl, 4-iodophenol, and stearyl alcohol were purchased from Tokyo Kasei Co. Ltd. Tantalum(V) pentachloride, *p*-*trans*-4-*n*-pentyl(cyclohexyl)phenol, *p*-(*trans*-4-*n*-pentylcyclohexyl)bromobenzene, *p*-pentyliodobenzene, and copper(I) iodide (CuI) were purchased from Kanto Chemical Co. Ltd. Triphenylphosphine (TPP), 10-undecyn-1-ol, and 25% ammonia ($NH_3$) solution were purchased from Wako Co. Ltd. Phenyl acetylene, sodium hydrogen carbonate ($NaHCO_3$), potassium carbonate ($K_2CO_3$), sodium sulfate ($Na_2SO_4$), triethylamine ($Et_3N$), tetrahydrofuran (THF), toluene, chloroform ($CHCl_3$), and acetone were purchased from Nacalai Tesque Co. Ltd. All experiments were performed under argon (>99.9995% purity) atmosphere. THF, $Et_3N$, and toluene used were distilled from sodium as a drying agent under argon gas before use.

**4.2. Methods.** Proton ($^1H$) and carbon ($^{13}C$) nuclear magnetic resonance (NMR) spectra were measured in chloroform-*d* using either a JEOL JNM EX400 400 MHz or a Bruker AVANCE-600 600 MHz NMR spectrometer. Chemical shifts are represented in parts per million downfield from tetramethylsilane (TMS) as an internal standard. Elemental analysis was measured using a Perkin-Elmer 2400 CHN elemental analyzer.

The microscope observation was carried out under crossed nicols using a Nikon ECLIPSE E400 POL POM equipped with a Nikon COOLPIX 950 digital camera and a Linkam TH600PM and L600 heating and cooling stage with temperature control. The samples for observations with POM were sandwiched between two cover glasses. Thermal behavior of the polymers was investigated in a heating run at a heating rate of 10 °C/min in flowing nitrogen gas, using thermogravimetry differential thermal analysis (TG-DTA) apparatus (TG-DTA6200, Seiko). The phase transition temperatures of monomers and polymers were determined using a Perkin-Elmer differential scanning calorimeter (DSC7) and a TA Instruments Q100 DSC apparatus at a constant heating and cooling rate of 10 °C/min, where first cooling and second heating were recorded.

Optical absorption spectra were measured using a Hitachi U-3500 spectrometer, and fluorescence spectra were measured using either JASCO FP-750 spectrometer or JASCO FP-6500 spectrometer with quartz cell (for solution) and quartz plate (for cast film). Fluorescence quantum yield of the polymers was measured in solution state using quinine sulfate as standard. Absolute fluorescence quantum yield of the polymers was measured in film state using integrating-sphere method at the JASCO FP-6500 spectrometer. Dichroic fluorescence spectra were obtained using polymer films after rubbing treatment. The polymers on the quartz substrates were heated to the LC temperature region, and these were rubbed with a glass rod. Then the polymer films were cooled to room temperature, yielding samples. During the cooling process of the polymers, LC textures remained unchanged even in glassy states. In the case of **PA4**, lyotropic LC solution in 10−15 wt % toluene was prepared, then applied to a quartz substrate, and then rubbed with a glass rod along the long axis.

Luminance and current−voltage curves were obtained with a Kollmorgen Instrument PR650 photospectrometer, a Kiethley model 2001 multimeter, and a Takasago GP050-2 dc voltage source. The EL configuration is shown in Figure 12a. The thin film of poly(3,4-ethylenedioxythiophene) (PEDOT)/poly(styrenesulfonate) (PSS) (hole transporting layer: HTL) was prepared by spin-coating on indium tin oxide (ITO: anode) substrate at a rotational speed of 1100 rpm from commercially available PEDOT/PSS solution annealed at 200 °C for 10 min. The polymer film (light emissive layer: LEL) was spin-coated at a rotational speed of 800 rpm from its toluene solution (1.5−2.5 wt %) filtered through 0.2 $\mu$m polytetrafluoroethylene (PTFE) filter and annealed at 90 °C for 1 h. The thickness of **PA1** and **PA2** was 83 and 91 nm, respectively (see Table 5). The layers of lithium fluoride (LiF) (electron injection layer: EIL), calcium (Ca) (electron transporting layer: ETL), and aluminum (Al) (cathode) were deposited in turn under vacuum ($9.2 \times 10^{-6}$−$1.2 \times 10^{-4}$ Pa). The thickness of LiF, Ca, and Al layers was 4, 5, and 81 nm, respectively (see Table S1). The conditions of vapor deposition of the EL layers are summarized in Supporting Information, Table S1.

The molecular weights of the polymers were determined by gel permeation chromatography (GPC) using a PLgel 5 $\mu$m MIXED-D

**Table 5. EL Characteristics of PA1 and PA2**

| | thickness (nm) | turn-on voltage (V) | $E_{m,max}$ (nm) | chromaticity coordinates ($x$, $y$) | max luminance (cd/m$^2$) | max current efficiency (cd/A) | max power efficiency (lm/W) |
|---|---|---|---|---|---|---|---|
| **PA1** | 83 | 6.9 | 480 | (0.26, 0.33) | 220 | 0.16 | 0.07 |
| **PA2** | 91 | 8.4 | 480 | (0.21, 0.30) | 50 | 0.24 | 0.08 |

(Polymer Laboratories), a JASCO MD915 UV detector, and THF as an eluent at a flow rate of 1.0 mL/min during measurements, where the instrument was calibrated using polystyrene (PS) standard, and were calculated on an 807-IT integrator.

XRD diffraction (XRD) measurements of the polymers were performed with a Rigaku ultra X18 diffractometer. XRD patterns were recorded with an X-ray generator with Nickel filtered Cu Kα radiation (40 kV/300 mA: $\lambda$ = 0.154 nm) and a flat plate camera (RINT2500, Rigaku). The polymers were heated up to isotropic state and then slowly cooled to room temperature via LC states, yielding XRD samples. Lyotropic LC samples for XRD measurements was prepared by first dissolving the polymer in toluene (10−15 wt % solution) to form a lyotropic LC phase. The lyotropic LC solution is then pulled up a XRD capillary tube (Hilgenberg Mark-tube glass #10, 0.01 mm wall thickness), yielding XRD samples. The diffraction pattern was recorded on an imaging plate and scanned by a R-AXIS DS3A imaging plate reader at 100 $\mu$m resolution.

**4.3. Syntheses of Monomers and Polymers.** The synthetic route of precursor compounds **1** to **9** are detailed in the Supporting Information. The syntheses of the LC-PA monomers (**M1**−**M7**) and LC-PAs (**PA1**−**PA7**) are given below:

*LC-PA Monomer 1 (**M1**).* **M1** was synthesized as follows. Into a 100 mL round-bottom flask were added 0.5 g (2.17 mmol) of compound **1**, 0.6 g of 4-bromo-4′-*n*-pentylbiphenyl (1.98 mmol), degassed 3 M aqueous $NaHCO_3$ (20 mL), and 40 mL of THF. After all the reagents were dissolved, the solution was heated to 80 °C and refluxed under constant stirring. TBA-OH (10 drops) and $(TPP)_4Pd$ (35 mg, 0.030 mmol) were then added. The solution was left stirring overnight and then cooled to room temperature; the layers were separated and washed with water and $CHCl_3$ (3×). The combined organic layers were dried over anhydrous $Na_2SO_4$, and the crude product was then purified by open column chromatography using $CHCl_3$ as eluent. The collected liquid was evaporated and dried under vacuum to give **M1** (0.78 mg, 1.91 mmol) as a greenish-white solid. Yield = 97%. Anal. Chemical Formula: $(C_{31}H_{36})_n$ (408.62)$_n$: Calcd C 91.12, H 8.88; Found C 91.31, H 8.98. $^1$H NMR (400 MHz, $CDCl_3$): $\delta$ = 0.89−0.93 (m, 6H, $-CH_3$), 1.33−1.37 (m, 8H, $-CH_2-$), 1.50−1.66 (s, 6H,$-CH_2-$), 2.43 (t, $J$ = 7.2 Hz, 2H, $-C_6H_6-CH_2-$), 2.65 (t, $J$ = 6.8 Hz, 2H, $-C_6H_6C{\equiv}CCH_2-$), 7.28 (d, 2H, $J$ = 4.4 Hz, Ar−H ortho to $-CH_2-$), 7.46 (d, 2H, $J$ = 8.4 Hz, Ar−H meta to $-CH_2-$), 7.54−7.68 (m, 8H, Ar−H). $^{13}$C NMR (400 MHz, $CDCl_3$): $\delta$ = 14.1, 19.5, 22.6, 28.6, 28.7, 30.7, 31.5, 35.1, 100.5, 123.0, 126.5, 126.7, 127.0, 127.2, 128.7, 131.8, 131.9, 138.0, 140.2, 179.1.

*LC-PA Monomer 2 (**M2**).* **M2** was synthesized as follows. Into a 100 mL round-bottom flask were added 0.96 g (4.1 mmol) of compound **1**, 2.01 g of compound **2** (2.5 mmol), degassed 3 M aqueous $NaHCO_3$ (20 mL), and 40 mL of THF. After all the reagents were dissolved, the solution was heated to 70 °C and refluxed under constant stirring. TBA-OH (10 drops) and $(TPP)_4Pd$ (75 mg, 0.067 mmol) were then added. The solution was left stirring overnight and then cooled to room temperature; the layers were then separated and washed with water and $CHCl_3$ (3×). The combined organic layers were dried over anhydrous $Na_2SO_4$, and the crude product was then purified by open column chromatography using $CHCl_3$ as eluent. The collected liquid was evaporated and dried under vacuum to give **M2** (0.85 mg, 1.4 mmol) as a colorless crystal. Yield = 35%. Anal. Chemical Formula: $(C_{44}H_{62}O)_n$ (606.48)$_n$: Calcd C 87.07, H 10.30, O 2.64; Found C 86.77, H 9.90. $^1$H NMR (600 MHz, $CDCl_3$): $\delta$ = 0.87−0.93 (m, 6H, $-CH_3$), 1.20−1.36 (m, 34H, $-CH_2-$), 1.45−1.50 (m, 4H, $-C{\equiv}CCH_2CH_2-$ and $-OCH_2CH_2$-$CH_2-$), 1.81 (m, 2H, $J$ = 25.6 Hz, $-OCH_2CH_2-$), 2.43 (t, 2H, $J$ = 10.5 Hz, $-C{\equiv}CCH_2$), 4.00 (t, 2H, $J$ = 13.1 Hz, $-OCH_2-$), 6.98 (d, 2H, $J$ = 8.8 Hz, Ar−H ortho to $-OCH_2-$), 7.40−7.63 (m, 10H, Ar−H). $^{13}$C NMR (600 MHz, $CDCl_3$): $\delta$ = 14.1, 19.5, 22.6, 22.7, 26.1, 28.6, 28.8, 29.3, 29.4, 29.6, 29.7, 31.4, 31.9, 68.1, 80.4, 91.3, 114.7, 123.0, 126.4, 126.7, 127.0, 127.8, 131.5, 132.8, 138.7, 139.7, 140.0, 158.9.

*LC-PA Monomer 3 (**M3**).* **M3** was synthesized as follows. Compound **3** (0.76 g, 2.70 mmol), *p*-(*trans*-4-*n*-pentylcyclohexyl)bromobenzene (0.75 g, 2.40 mmol), degassed 3 M aqueous $NaHCO_3$ (20 mL), and 40 mL of THF were added into a 100 mL round-bottom flask. The solution was heated to 80 °C and refluxed under constant stirring. TBA-OH (10 drops) and $(TPP)_4Pd$ (42 mg, 0.036 mmol) were then added. The solution was left stirring overnight and then cooled to room temperature; the layers were then separated and washed with water and $CHCl_3$ (3×). The combined organic layers were dried over anhydrous $Na_2SO_4$, and the crude product was then purified by open column chromatography using $CHCl_3$ as eluent. The collected liquid was evaporated and dried under vacuum to give **M3** (1.06 g, 2.2 mmol) as a greenish-white solid. Yield = 93%. Anal. Chemical Formula: $(C_{35}H_{50})_n$ (464.72)$_n$: Calcd C 89.29, H 10.71; Found C 86.38, H 10.53. $^1$H NMR (400 MHz, $CDCl_3$): $\delta$ = 0.85−0.90 (m, 6H, $-CH_3$), 1.00−1.45 (m, 25H, Ar−$CH(CH_2)_4CH-(CH_2)_4-$, Ar−$C{\equiv}C-CH_2CH_2(CH_2)_7-$, and Ar−$CH(CH_2)_3CH_2CH-C_5H_{11}$), 1.48−1.60 (m, 6H, Ar−$CH(CH_2)_3CH_2CH-C_5H_{11}$), 1.83−1.92 (m, 3H, Ar−$C{\equiv}C-CH_2CH_2-$ and Ar−$CH(CH_2)_4CH-$), 2.40 (t, 2H, $J$ = 7.2 Hz, Ar−$C{\equiv}C-CH_2-$), 7.06 (d, 2H, $J$ = 8.4 Hz, Ar−H ortho to $-C_6H_{10}-C_5H_{11}-$), 7.37 (d, 2H, $J$ = 8.4 Hz, Ar−H meta to $-C_6H_{10}-C_5H_{11}-$), 7.42 (d, 2H, $J$ = 8.8 Hz, Ar−H meta to $-C{\equiv}C-C_{10}H_{21}$), 7.48 (d, 2H, $J$ = 8.8 Hz, Ar−H ortho to $-C{\equiv}C-C_{10}H_{21}$). $^{13}$C NMR (400 MHz, $CDCl_3$): $\delta$ = 14.1, 22.7, 26.6, 28.8, 28.9, 29.2, 29.3, 29.6, 31.9, 32.2, 33.6, 34.3, 37.4, 44.3, 80.4, 104.0, 122.6, 126.7, 127.1, 128.4, 131.7, 137.9, 140.0, 145.8.

*LC-PA Monomer 4 (**M4**).* **M4** was synthesized as follows. Into a 100 mL round-bottom flask, 0.50 g (2.25 mmol) of compound **4**, 0.62 g (2.00 mmol) of 4-bromo-4′-*n*-pentylbiphenyl, degassed 3 M aqueous $NaHCO_3$ (20 mL), and 40 mL of THF were added under an argon atmosphere. The solution was stirred, heated to 80 °C, and refluxed for 30 min. TBA-OH (10 drops) and $(TPP)_4Pd$ (35 mg, 0.03 mmol) were then added. The solution was left stirring overnight and then cooled to room temperature; the layers were then washed with water and were extracted using $CHCl_3$ (3×). The combined organic layers were dried over anhydrous $Na_2SO_4$, and the crude product was then purified by open column chromatography using $CHCl_3$ as eluent. The collected liquid was evaporated and dried under vacuum to give **M4** (0.58 g, 1.40 mmol) as a yellowish-white solid. Yield = 70%. Anal. Chemical Formula: $(C_{31}H_{28})_n$ (400.55)$_n$: Calcd C, 92.95; H, 7.05; Found C 93.17, H 7.00. $^1$H NMR (400 MHz, $CDCl_3$): $\delta$ = 0.91 (t, 3H, $J$ = 7.2 Hz, $-CH_3$), 1.34−1.38 (m, 4H, Ar−$(CH_2)_2(CH_2)_2CH_3$), 1.51−1.69 (m, 2H, Ar−$CH_2CH_2(CH_2)_2CH_3$), 2.66 (t, 2H, $J$ = 8 Hz, Ar−$CH_2(CH_2)_3CH_3$), 7.23−7.36 (m, 4H, $-C{\equiv}C-C_6H_4C_6H_4C_6H_4-C_5H_{11}$), 7.54−7.70 (m, 13H, $C_6H_5-C{\equiv}C-$, $-C{\equiv}C-C_6H_4-$, and $-C{\equiv}C-(C_6H_4)_2C_6H_4-C_5H_{11}$). $^{13}$C NMR (400 MHz, $CDCl_3$): $\delta$ = 14.0, 22.5, 31.1, 31.5, 56.0, 89.3, 122.0, 126.7, 127.1, 128.2, 128.8, 131.5, 131.9, 137.7, 140.3.

*LC-PA Monomer 5 (**M5**).* **M5** was synthesized as follows. TPP (1.86 g, 7.10 mmol) and *p-trans*-4-*n*-pentyl(cyclohexyl)phenol (1.60 g, 6.45 mmol) were added under argon gas into a 300 mL three-necked flask, dissolved in THF (60 mL), and then stirred. In the addition funnel, a mixture of DEAD (3.09 g, 40 wt % in toluene, 7.10 mmol), compound **5** (2.40 g, 7.70 mmol), and 20 mL of THF was prepared. After dissolving the reagents under constant stirring, the flask was placed in an ice bath and the THF solution in the addition funnel was added dropwise to the solution in the flask. The solution was left overnight at room temperature. TLC indicated completion of the reaction. After evaporation of the solvent, the residue was washed with water and extracted with $CHCl_3$ (3×). The residue was dried over anhydrous $Na_2SO_4$, and the crude product was then purified by open column chromatography using $CHCl_3$ as eluent. The product was recrystallized from *n*-hexane and dried under vacuum to give 2.36 g (4.3 mmol) of **M5** as a white crystal. Yield = 67%. Anal. Chemical Formula: $(C_{39}H_{58}O)_n$ (542.88)$_n$: Calcd C, 86.28; H, 10.77; O, 2.95; Found C 86.41, H 10.83. $^1$H NMR (400 MHz, $CDCl_3$): $\delta$ = 0.83−0.91 (m, 6H, $J$ = 7.2 Hz, $-CH_3$), 1.00−1.61 (m, 28H, $-C\equiv C-Ar-CH_2(CH_2)_3CH_3$, $Ar-C\equiv C-CH_2(CH_2)_7CH_2O-$, $Ar-C_6H_{10}-(CH_2)_4CH_3$), 1.71−1.87 (m, 9H, $Ar-CH(CH_2)_4CH-C_5H_{11}$), 2.35−2.39 (m, 3H, $-C\equiv C-Ar-CH_2-(CH_2)_3CH_3$, and $Ar-CH(CH_2)_4CH-C_5H_{11}$), 2.55 (t, 2H, $J$ = 7.6 Hz, $-Ar-C\equiv C-CH_2-$), 3.90 (t, 2H, $J$ = 6.8 Hz, $Ar-O-CH_2-$), 6.80 (d, 2H, $J$ = 8.4 Hz, Ar−H ortho to $-(CH_2)_9-O$), 7.04−7.10 (m, 2H, Ar−H meta to $-(CH_2)_9-O$, and Ar−H meta to $-(CH_2)_9-C\equiv C-$), 7.28 (d, 2H, $J$ = 8.4 Hz, Ar−H, ortho to $-(CH_2)_9-C\equiv C-$). $^{13}$C NMR (400 MHz, $CDCl_3$): $\delta$ = 14.1, 22.7, 26.0, 26.6, 28.8, 29.1, 29.3, 30.9, 31.4, 32.2, 35.7, 43.7, 67.9, 80.5, 108.1, 114.1, 127.4, 128.1, 131.2, 139.7, 142.2, 157.0.

*LC-PA Monomer 6 (**M6**).* **M6** was synthesized as follows. Into a 100 mL three-necked flask, TPP (0.87 g, 3.3 mmol) and compound **7** (0.58 g, 3.0 mmol) were added under argon gas, dissolved in THF (15 mL), and then stirred. In the addition funnel, a mixture of DEAD (1.44 g, 40 wt % in toluene, 3.3 mmol), compound **6** (1.42 g, 3.3 mmol), and 5 mL of THF was prepared. After dissolving the reagents under constant stirring, the flask was placed in an ice bath and the THF solution in the addition funnel was added dropwise to the solution in the flask. The solution was left overnight at room temperature. TLC indicated completion of the reaction. After evaporation of the solvent, the residue was washed with water and extracted with $CHCl_3$ (3×). The residue was dried over anhydrous $Na_2SO_4$, and the crude product was then purified by open column chromatography using $CHCl_3$ as eluent. The product was recrystallized from *n*-hexane and dried under vacuum to give 1.56 g (2.6 mmol) of **M6** as a white crystal. Yield = 85%. Anal. Chemical Formula: $(C_{43}H_{58}O_2)_n$ (606.92)$_n$: Calcd C, 85.10; H, 9.63; O, 5.27; Found C 85.25, H 9.63. $^1$H NMR (400 MHz, $CDCl_3$): $\delta$ = 0.89 (t, 3H, $J$ = 7.6 Hz, $-C_6H_{10}-(CH_2)_4CH_3$), 0.97−1.08 (m, 2H, $-C_6H_{10}-(CH_2)_3CH_2CH_3$), 1.11−1.45 (m, 27H, $-C\equiv C-Ar-O-CH_2(CH_2)_{10}-CH_2-$, and $-Ar-CH(CH_2)_4CH(CH_2)_3CHCH_3-$), 1.72−1.86 (m, 8H, $-O-Ar-CH(CH_2)_4CH-C_5H_{11}-$), 2.40 (m, 1H, $-O-Ar-CH(CH_2)_4-CH-C_5H_{11}-$), 3.94 (m, 4H, $Ar-O-CH_2(CH_2)_{10}CH_2-O-Ar$), 6.80−6.88 (m, 4H, Ar−H meta to Ar−C≡C−, and Ar−H meta to $-C_6H_{10}-C_5H_{11}$), 7.10 (d, 2H, $J$ = 8.4 Hz, Ar−H ortho to $-C_6H_{10}C_5H_{11}$), 7.30−7.35 (m, 3H, Ar−H meta and para to $-C\equiv C-Ar-O-C_{12}H_{24}-$), 7.44−7.52 (m, 4H, Ar−H ortho to $-C\equiv C-$). $^{13}$C NMR (400 MHz, $CDCl_3$): $\delta$ = 14.1, 22.7, 26.0, 26.6, 29.5, 30.4, 32.2, 33.0, 37.3, 43.7, 68.0, 87.8, 114.1, 114.4, 127.4, 128.1, 131.3, 132.9, 139.8, 157.0, 159.1.

*LC-PA Monomer 7 (**M7**).* **M7** was synthesized as follows. The reagents compound **8** (1.1 g, 1.7 mmol), compound **9** (0.6 g, 1.7 mmol), $PdCl_2(TPP)_2$ (24.4 mg, 0.35 mmol), CuI (13.2 mg, 0.70 mmol), 25 mL of $Et_3N$, and 10 mL of THF were added under an argon atmosphere into a 200 mL three-necked flask. The solution was stirred and heated to 65 °C overnight under an argon atmosphere. TLC indicated completion of the reaction. After evaporation of the solvent, the residue was thoroughly washed with water and extracted with $CHCl_3$ (3×). The organic layer was dried over anhydrous $Na_2SO_4$. The solution was evaporated and purified by open column chromatography (silica gel, hexane/ethyl acetate = 1:1). The product was recrystallized from ethanol and dried in vacuo to give 0.95 g (1.0 mmol) of **M7** as a white powder. Yield = 61%. Anal. Chemical Formula: $(C_{63}H_{96}O_3)_n$ (901.43)$_n$: Calcd C, 83.94; H, 10.73; O, 5.32; Found C 83.88, H 10.74. $^1$H NMR (400 MHz, $CDCl_3$): $\delta$ = 0.87−0.91 (m, 6H, $-C_6H_{10}-(CH_2)_4CH_3$), 0.97−1.08 (m, 4H, $-C_6H_{10}-(CH_2)_3CH_2CH_3$), 1.20−1.86 (m, 64H, $-O-Ar-CH(CH_2)_4CH(CH_2)_3CH_3$, $-C\equiv C-Ar-O-CH_2(CH_2)_{10}-CH_2-O-$, and $-C\equiv C-CH_2(CH)_7CH_2-O-$), 2.35−2.43 (m, 4H, $Ar-CH(CH_2)_4CH_2-C_5H_{11}$, and $-O-(CH_2)_8CH_2-C\equiv C-Ar$), 3.90−3.93 (m, 6H, $-C\equiv C-Ar-O-CH_2(CH_2)_{10}CH_2-O-$, and $-O-CH_2(CH_2)_8-C\equiv C-Ar-$), 6.78−6.82 (m, 6H, Ar−H meta to $-C_6H_{10}-C_5H_{11}$ and meta to $-C\equiv C-(CH_2)_9-O-$), 7.09−7.11 (m, 4H, Ar−H ortho to $-C_6H_{10}C_5H_{11}$), 7.30 (d, 2H, $J$ = 8.8 Hz, ortho to $-C\equiv C-(CH_2)_9-O-$). $^{13}$C NMR (400 MHz, $CDCl_3$): $\delta$ = 14.1, 22.7, 26.0, 26.7, 28.9, 29.5, 32.2, 33.7, 34.6, 36.4, 37.3, 37.4, 43.7, 67.9, 80.3, 101.4, 114.1, 114.2, 127.4, 132.6, 134.2, 139.8, 157.1, 160.1.

*LC-PA1 (**PA1**).* **PA1** was synthesized as follows. Toluene (1.5 mL), $TaCl_5$ (36 mg, 0.1 mmol), and *n*-$Bu_4Sn$ (36 mg, 0.1 mmol) were added under argon into a Schlenk flask. The catalyst mixture was stirred at 80 °C for 30 min, and then **M1** (0.42 g, 1 mmol) was dissolved in 1 mL of toluene and was then added to the reaction mixture. The reaction mixture was stirred at 80 °C for 24 h. The mixture was cooled to room temperature and was added dropwise to 800 mL of methanol (MeOH) under stirring. The polymer precipitate stirred for 24 h, which was then filtered and washed again in 800 mL of acetone. After 24 h, the polymer was filtered, washed with acetone, and dried in a vacuum oven. A greenish-white powder was obtained with a yield of 84% (0.35 g, 0.84 mmol). $M_w$ = 190 000 $M_w/M_n$ = 2.8 (GPC, polystyrene calibration). Anal. Chemical Formula: $(C_{31}H_{36})_n$ (408.62)$_n$: Calcd C 91.12, H 8.88; Found C 87. 56, H 8.53. $^1$H NMR (600 MHz, $CDCl_3$): $\delta$ = 0.63−2.46 (br, 24H, $-CH_2-$ and $-CH_3$), 6.56−7.63 (br, 12H, −Ar−H). $^{13}$C NMR (600 MHz, $CDCl_3$): $\delta$ = 14.2, 22.7, 26.7, 29.2, 29.5, 30.0, 30.2, 31.8, 32.2, 33.7, 34.1, 34.4, 37.4, 44.3, 125.5, 126.7, 127.0, 128.2, 128.7, 129.5, 129.9, 140.0, 146.5.

*LC-PA2 (**PA2**).* **PA2** was synthesized in a similar way as **PA1**. Polymerization of **M2** (0.61 g, 1 mmol) yielded a greenish powder with a yield of 56% (0.34 g, 0.56 mmol). $M_w$ = 409 000; $M_w/M_n$ = 2.4 (GPC, polystyrene calibration). Anal. Chemical Formula: $(C_{44}H_{62}O)_n$ (606.48)$_n$: Calcd C 87.07, H 10.30; Found C 86.06, H 9.85. $^1$H NMR (600 MHz, $CDCl_3$): $\delta$ = 0.77−0.91 (br, 6H, $-CH_3$), 1.26−1.48 (br, 34H, $-CH_2-$), 1.77−1.83 (br, 4H, $-C\equiv CCH_2CH_2-$ and $-OC-H_2CH_2-$), 3.90−4.02 (br, 2H, $-OCH_2-$), 6.89−7.66 (br, 12H, Ar−H). $^{13}$C NMR (600 MHz, $CDCl_3$): $\delta$ = 14.1, 22.7, 26.1, 29.4, 29.7, 30.3, 31.9, 68.1, 114.8, 125.9, 126.3, 126.7, 126.8, 127.0, 127.1, 127.3, 128.0, 132.0, 138.7, 139.1.

*LC-PA3 (**PA3**).* **PA3** was synthesized in a similar way as **PA1**. Polymerization of **M3** (0.30 g, 0.6 mmol) yielded a greenish-yellow solid with a yield of 51% (0.15 g, 0.31 mmol). $M_w$ = 267 000; $M_w/M_n$ = 3.3 (GPC, polystyrene calibration). Anal. Chemical Formula: $(C_{35}H_{50})_n$ (470.77)$_n$: Calcd C 89.29, H 10.71; Found C 83.12, H 9.95. $^1$H NMR (400 MHz, $CDCl_3$): $\delta$ = 0.81−3.65 (br, 42H, $-CH$, $-CH_2-$, and $-CH_3$), 6.21−7.71 (br, 8H, Ar−H). $^{13}$C NMR (400 MHz, $CDCl_3$): $\delta$ = 14.1, 22.7, 26.7, 29.7, 34.3, 37.3, 44.1, 110.9, 114.8, 122.1, 126.8, 148.9, 152.4.

*LC-PA4 (**PA4**).* **PA4** was synthesized in a similar way as **PA1**. Polymerization of **M4** (0.40 g, 1 mmol) yielded a yellow solid with a yield of 33% (0.13 g, 0.33 mmol). $M_w$ = 302 000; $M_w/M_n$ = 3.4 (GPC, polystyrene calibration). Anal. Chemical Formula: $(C_{31}H_{28})_n$ (400.55)$_n$: Calcd C 92.95, H 7.05; Found C 87.43, H 7.15. $^1$H NMR (400 MHz, $CDCl_3$): $\delta$ = 0.80−1.00 (br, 3H, $-CH_3$), 1.23−3.94 (br, 8H, $-CH_2-$), 7.22−7.79 (br, 17H, Ar−H). $^{13}$C NMR (400 MHz, $CDCl_3$): $\delta$ = 16.4, 28.0, 34.2, 43.1, 50.1, 54.4, 58.8, 80.2, 88.7, 93.8, 104.5, 146.0, 152.4, 156.6, 164.7.

*LC-PA5* (***PA5***). **PA5** was synthesized in a similar way as **PA1**. Polymerization of **M5** (0.35 g, 0.6 mmol) yielded a white powder with a yield of 12% (42 mg, 0.07 mmol). $M_w$ = 168 000; $M_w/M_n$ = 2.6 (GPC, polystyrene calibration). Anal. Chemical Formula: $(C_{39}H_{58}O)_n$ $(542.88)_n$: Calcd C 86.28, H 10.77, O 2.95; Found C 81.82, H 11.03. $^1$H NMR (400 MHz, $CDCl_3$): $\delta$ = 0.80−0.90 (br, 6H, $-CH_3$), 1.00−1.98 (br, 37H, $-C{\equiv}C-Ar-CH_2(CH_2)_3CH_3$, $Ar-C{\equiv}C-CH_2-(CH_2)_7CH_2O-$, $Ar-C_6H_{10}-(CH_2)_4CH_3$, and $Ar-CH(CH_2)_4CH-C_5H_{11}$), 2.07−2.68 (br, 5H, $-C{\equiv}C-Ar-CH_2(CH_2)_3CH_3$, $Ar-CH-(CH_2)_4CH-C_5H_{11}$, and $-Ar-C{\equiv}C-CH_2-$), 3.68−3.95 (br, 2H, $Ar-O-CH_2-$), 6.64−7.51 (br, 8H, Ar−H). $^{13}$C NMR (400 MHz, $CDCl_3$): $\delta$ = 14.1, 22.7, 26.7, 31.3, 32.3, 33.7, 37.3, 43.7, 67.8, 93.3, 114.1, 127.3, 139.5, 157.1.

*LC-PA6* (***PA6***). **PA6** was synthesized in a similar way as **PA1**. Polymerization of **M6** (0.30 g, 0.5 mmol) yielded a green solid with a yield of 45% (0.14 g, 0.23 mmol). $M_w$ = 367 000; $M_w/M_n$ = 1.7 (GPC, polystyrene calibration). Anal. Chemical Formula: $(C_{43}H_{58}O_2)_n$ $(606.92)_n$: Calcd C 85.10, H 9.63, O 5.27; Found C 85.25, H 9.63. $^1$H NMR (400 MHz, $CDCl_3$): $\delta$ = 0.32−0.51 (br, 3H, $-CH_3$), 0.80−2.17 (br, 37H, $-O-Ar-CH(CH_2)_4CH-C_5H_{11}-$, $-Ar-CH(CH_2)_4CH-(CH_2)_3CHCH_3-$, $-C_6H_{10}-(CH_2)_3CH_2CH_3$, and $-C{\equiv}C-Ar-O-CH_2(CH_2)_{10}CH_2-$), 2.40 (br, 1H, $-O-Ar-CH(CH_2)_4CH-C_5H_{11}-$), 3.19−3.83 (br, 4H, $Ar-O-CH_2(CH_2)_{10}CH_2-O-Ar$), 6.91−7.71 (br, 13H, Ar−H). $^{13}$C NMR (400 MHz, $CDCl_3$): $\delta$ = 13.3, 18.3, 26.6, 42.0, 52.4, 54.9, 68.4, 83.3, 89.4, 92.7, 102.4, 110.6, 117.1, 147.0, 150.6, 152.5, 162.7, 175.5.

*LC-PA7* (***PA7***). **PA7** was synthesized in a similar way as **PA1**. Polymerization of **M7** (0.5 g, 0.6 mmol) yielded a yellow solid with a yield of 66% (0.33 g, 0.33 mmol). $M_w$ = 89 000; $M_w/M_n$ = 4.5 (GPC, polystyrene calibration). Anal. Chemical Formula: $(C_{63}H_{96}O_3)_n$ $(901.43)_n$: Calcd C 83.94, H 10.73, O 5.32; Found C 80.94, H 10.73 $^1$H NMR (400 MHz, $CDCl_3$): $\delta$ = 0.78−0.94 (br, 6H, $-C_6H_{10}-(CH_2)_4CH_3$), 0.96−1.09 (br, 4H, $-C_6H_{10}-(CH_2)_3CH_2CH_3$), 1.18−2.81 (br, 64H, $-O-Ar-CH(CH_2)_4CH(CH_2)_3CH_3$, $-C{\equiv}C-Ar-O-CH_2(CH_2)_{10}CH_2-O-$, and $-C{\equiv}C-CH_2(CH)_7CH_2-O-$), 2.35−2.43 (m, 4H, $Ar-CH(CH_2)_4CH_2-C_5H_{11}$, and $-O-(CH_2)_8-CH_2-C{\equiv}C-Ar$), 3.49−3.83 (br, 6H, $-C{\equiv}C-Ar-O-CH_2(CH_2)_{10}-CH_2-O-$, and $-O-CH_2(CH_2)_8-C{\equiv}C-Ar-$), 6.56−6.76 (br, 6H, Ar−H meta to $-C_6H_{10}C_5H_{11}$ and meta to $-C{\equiv}C-(CH_2)_9-O-$), 6.80−7.19 (br, 4H, Ar−H ortho to $-C_6H_{10}C_5H_{11}$), 7.20−7.26 (br, 2H, ortho to $-C{\equiv}C-(CH_2)_9-O-$). $^{13}$C NMR (400 MHz, $CDCl_3$): $\delta$ = 14.1, 22.7, 28.5, 30.9, 33.7, 34.6, 37.4, 43.8, 67.8, 101.5, 114.2, 127.5, 128.3, 135.8, 151.5, 157.3, 159.8.

## ■ ASSOCIATED CONTENT

**Supporting Information.** Synthetic routes of the precursor compounds, monomers, and polymers, representative results of thermogravimetry−differential thermal analysis (TG-DTA), differential scanning calorimeter (DSC) measurement, X-ray diffraction (XRD), optical properties of the monomers, conditions of vapor deposition for the EL device, and EL characteristics of the polymers. This material is available free of charge via the Internet at http://pubs.acs.org.

## ■ AUTHOR INFORMATION

**Corresponding Author**
*E-mail: akagi@fps.polym.kyoto-u.ac.jp.

## ■ ACKNOWLEDGMENT

The authors give thanks to Dr. Jun Oguma (Sumitomo Chemical, Japan) for the measurements of EL properties of the polymers. This work was supported by a Grant-in-Aid for Science Research (S) (No. 20225007) from the Ministry of Education, Culture, Sports, Science and Technology, Japan.

## ■ REFERENCES

(1) (a) Naarrmann, H.; Theophilou, N. *Synth. Met.* **1987**, *22*, 1–8. (b) Akagi, K.; Suezaki, M.; Shirakawa, H.; Kyotani, H.; Shimomura, M.; Tanabe, Y. *Synth. Met.* **1989**, *28*, D1–D10. (c) Tsukamoto, J.; Takahashi, A.; Kawasaki, K. *Jpn. J. Appl. Phys.* **1990**, *29*, 125–130.

(2) (a) Burroughes, J. H.; Bradley, D. C. C.; Brown, A. R.; Marks, R. N.; Mackay, K.; Friend, R. H.; Burns, P. L.; Holmes, A. B. *Nature* **1990**, *347*, 539–541. (b) Gustafsson, G.; Cao, Y.; Treacy, G. M.; Klavetter, F.; Colaneri, N.; Heeger, A. J. *Nature* **1992**, *357*, 477–479. (c) Burn, P. L.; Holmes, A. B.; Kraft, A.; Bradley, D. C. C.; Brown, A. R.; Friend, R. H.; Gymer, R. W. *Nature* **1992**, *356*, 47–49. (d) Grem, G.; Lditzky, G.; Ulrich, B.; Leising, G. *Adv. Mater.* **1992**, *4*, 36–37. (e) Greenham, N. C.; Moratti, S. C.; Bradley, D. D. C.; Friend, R. H.; Holmes, A. B. *Nature* **1993**, *365*, 628–630. (f) Kraft, A.; Grimsdale, A. C.; Holmes, A. B. *Angew. Chem., Int. Ed.* **1998**, *37*, 402–428. (g) Katz, H. E.; Bao, Z.; Gilat, S. L. *Acc. Chem. Res.* **2001**, *34*, 359–369.

(3) (a) Shacklette, L. W.; Eckhardt, H.; Chance, R. R.; Miller, G. G.; Ivory, D. M.; Baughman, R. H. *J. Chem. Phys.* **1980**, *73*, 4098–4102. (b) McCullough, R. D.; Tristramnagle, S.; Williams, S. P.; Lowe, R. D.; Jayaraman, M. *J. Am. Chem. Soc.* **1993**, *115*, 4910–4911. (c) Marks, R. N.; Halls, J. J. M.; Bradley, D. D. C.; Friend, R. H.; Holmes, A. B. *J. Phys.: Condens. Matter* **1994**, *6*, 1379–1394. (d) Halls, J. J. M.; Walsh, C. A.; Greenham, N. C.; Marseglia, E. A.; Friend, R. H.; Moratti, S. C. *Nature* **1995**, *376*, 498–500. (e) Tessler, N.; Denton, G. J.; Friend, R. H. *Nature* **1996**, *382*, 695–697. (f) Sirringhaus, H.; Tessler, N.; Friend, R. H. *Science* **1998**, *280*, 1741–1744.

(4) Suga, T.; Konishi, H.; Nishide, H. *Chem. Commun.* **2007**, 1730–1732.

(5) (a) Sariciftci, N. S.; Braun, D.; Zhang, C.; Srdanov, V. I.; Heeger, A. J.; Stucky, G.; Wudl, F. *Appl. Phys. Lett.* **1993**, *62*, 585–587. (b) Yu, G.; Heeger, A. *J. Appl. Phys.* **1995**, *78*, 4510–4515. (c) Granstrom, M.; Petritsch, K.; Arias, A. C.; Lux, A.; Andersson, M. R.; Friend, R. H. *Nature* **1998**, *395*, 257–260. (d) Daubler, T. K.; Glowacki, I.; Scherf, U.; Ulanski, J.; Horhold, H.-H.; Neher, D. *J. Appl. Phys.* **1999**, *86*, 6915–6923. (e) Huynh, W. U.; Dittmer, J. J.; Alivisatos, A. P. *Science* **2002**, *295*, 2425–2427. (f) Coakley, K. M.; McGehee, M. D. *Chem. Mater.* **2004**, *16*, 4533–4542.

(6) (a) Trepka, W. J.; Sonnenfeld, R. J. *J. Polym. Sci.* **1970**, *8*, 2721–2724. (b) Kern, R. J. *J. Polym. Sci.* **1969**, *7*, 621–631. (c) Simionescu, C. I.; Percec, V. *J. Polym. Sci., Polym. Symp.* **1980**, *67*, 43–71.

(7) (a) Oh, S. Y.; Akagi, K.; Shirakawa, H. *Macromolecules* **1993**, *26*, 6203–6206. (b) Ting, C.-H.; Chen, J.-T.; Hsu, C.-S. *Macromolecules* **2002**, *35*, 1180–1189. (c) Liu, K.-P.; Yu, Z.-Q.; Liu, J.-H.; Chen, E.-Q. *Macromol. Chem. Phys.* **2009**, *210*, 707–716. (d) Koltzenburg, S.; Wolff, D.; Stelzer, F.; Springer, J.; Nuyken, O. *Macromolecules* **1998**, *26*, 9166–9173. (e) Choi, S. K.; Gal, Y. S.; Jin, S. H.; Kim, H. K. *Chem. Rev.* **2000**, *100*, 1645–1682. (f) Chen, Y.; Chen, L.; Zhou, W.; Zha, D.; Zhou, D.; Bai, F.; Wan, M. *Synth. Met.* **2009**, *159*, 1649–1656.

(8) (a) Akagi, K.; Oguma, J.; Shirakawa, H. *J. Photopolym. Sci. Technol.* **1998**, *11*, 249–252. (b) Akagi, K.; Oguma, J.; Shibata, S.; Toyoshima, R.; Osaka, I.; Shirakawa, H. *Synth. Met.* **1999**, *102*, 1287–1288. (c) Oguma, J.; Kawamoto, R.; Goto, H.; Itoh, K.; Akagi, K. *Synth. Met.* **2001**, *119*, 537–538. (d) Oguma, J.; Akagi, K.; Shirakawa, H. *Synth. Met.* **1999**, *101*, 86–87. (e) Oguma, J.; Dai, X.-M.; Akagi, K. *Mol. Cryst. Liq. Cryst.* **2001**, *365*, 331–338. (f) Suda, K.; Yoshida, J.; Nimori, S.; Akagi, K. *Synth. Met.* **2009**, *159*, 943–948.

(9) Akagi, K. *Bull. Chem. Soc. Jpn.* **2007**, *80*, 649–661.

(10) Akagi, K. Liquid Crystalline Conjugated Polymers Synthesis and Properties. In *Thermotropic Liquid Crystals: Recent Advances*; Ramamoorthy, A., Ed.; Springer: Dordrecht, The Netherlands, 2007; Chapter 9, pp 249−275.

(11) (a) Akagi, K.; Tanaka, H.; Toyoshima, R.; Shirakawa, H. *Trans. Mater. Res. Soc. Jpn.* **1994**, *15A*, 513. (b) Toyoshima, R.; Narita, M.;

Akagi, K.; Shirakawa, H. *Synth. Met.* **1995**, *69*, 289–290. (c) Koide, N.; Iida, H. *Mol. Cryst. Liq. Cryst.* **1995**, *261*, 427–436. (d) Toyoshima, R.; Akagi, K.; Shirakawa, H. *Synth. Met.* **1997**, *84*, 431–432. (e) Akagi, K.; Narita, M.; Toyoshima, R.; Shirakawa, H. *Mol. Cryst. Liq. Cryst.* **1998**, *318*, 157–178.(f) Akagi, K. Liquid Crystalline and Electroresponsive Polythiophenes. In *Handbook of Thiophene-Based Materials: Applications in Organic Electronics and Photonics*; Perepichka, I. F., Perepichka, D. F., Eds.; John Wiley Sons: New York, 2009; Chapter 12, pp 497−515.

(12) (a) Vicentini, F.; Barrouillet, J.; Laversanne, R.; Mauzac, M.; Bibonne, F.; Parneix, J. P. *Liq. Cryst.* **1995**, *19*, 235–240. (b) Ibison, P.; Foot, P. J. S.; Brown, W. *Synth. Met.* **1996**, *76*, 297–300.

(13) (a) Osaka, I.; Shibata, S.; Toyoshima, R.; Akagi, K.; Shirakawa, H. *Synth. Met.* **1999**, *102*, 1437–1438. (b) Osaka, I.; Goto, H.; Itoh, K.; Akagi, K. *Synth. Met.* **2001**, *119*, 541–542. (c) Osaka, I.; Goto, H.; Itoh, K.; Akagi, K. *Mol. Cryst. Liq. Cryst.* **2001**, *365*, 339–346.

(14) (a) Goto, H.; Itoh, K.; Akagi, K. *Synth. Met.* **2001**, *119*, 351–352. (b) Goto, H.; Akagi, K. *Macromolecules* **2002**, *35*, 2545–2551.

(15) (a) Shukla, A.; Mazumdar, S. *Phys. Rev. Lett.* **1999**, *19*, 3944–3947. (b) Hidayat, R.; Fujii, A.; Ozaki, M.; Teraguchi, M.; Masuda, T.; Yoshino, K. *Synth. Met.* **2001**, *119*, 597–598. (c) Shukla, A.; Ghosh, H.; Mazumdar, S. *Synth. Met.* **2001**, *116*, 87–90. (d) Ghosh, H.; Shukla, A.; Mazumdar, S. *Phys. Rev. B* **2000**, *19*, 12763–12774. (e) Vardeny, Z. V., Korovyanko, O. In *Handbook of Conducting Polymers, Conjugated Polymers*, 3rd ed.; Skotheim, T. A., Reynolds, J. R., Eds.; CRC Press: New York, 2007; pp 22-1−22-74.

(16) Excitons are formed during the photoexcitation of the electron to the lowest unoccupied molecular orbital (LUMO) and the vacating of a hole in the highest occupied molecular orbital (HOMO). This electron−hole pair is bound together by Coulombic attraction. During the radiative recombination of excitons, the excited electron drops down to the ground state and combines with the paired hole to release a photon. Upon the formation of excitons, the radiative recombination of excitons occurs in the order of nanoseconds. During this time scale, the excitons have already been delocalized into the phenyl side chains; thus, the radiative recombination occurs at the phenyl side chains.

(17) (a) Lam, J. W. Y.; Tang, B. Z. *J. Polym. Sci., Part A: Polym. Chem.* **2003**, *41*, 2607. (b) Liu, J.; Lam, J. W. Y.; Tang, B. Z. *Chem. Rev.* **2009**, *109*, 5799–5867. (c) Yang, S.-H.; Huang, C.-H.; Chen, C.-H.; Hsu, C.-S. *Macromol. Chem. Phys.* **2009**, *210*, 37–47. (d) Peng, H.; Chen, Y.; Chen, L.; He, X.; Li, F. *J. Polym. Sci., Part A: Polym. Chem.* **2010**, *48*, 5679–5692.

(18) (a) Kwak, G.; Minakuchi, M.; Sakaguchi, T.; Masuda, T.; Fujiki, M. *Chem. Mater.* **2007**, *19*, 3654–3661. (b) Kwak, G.; Fukao, S.; Fujiki, M.; Sakaguchi, T.; Masuda, T. *Chem. Mater.* **2006**, *18*, 5537–5542. (c) Kwak, G.; Minakuchi, M.; Sakaguchi, T.; Masuda, T.; Fujiki, M. *Macromolecules* **2008**, *41*, 2743–2746. (d) Lee, W-.E.; Kim, J-.W.; Oh, C-.J.; Sakaguchi, T.; Fujiki, M.; Kwak, G. *Angew. Chem., Int. Ed.* **2010**, *49*, 1406–1409.

(19) Iida, H.; Nakamura, A.; Inoue, Y.; Akagi, K. *Synth. Met.* **2003**, *135*, 91–92.

(20) Suda, K.; Akagi, K. *J. Polym. Sci., Part A: Polym. Chem.* **2008**, *46*, 3591–3610.

(21) (a) Hayasaka, H.; Tamura, K.; Akagi, K. *Macromolecules* **2008**, *41*, 2341–2346. (b) Hayasaka, H.; Miyashita, T.; Tamura, K.; Akagi, K. *Adv. Funct. Mater.* **2010**, *20*, 1243–1250.

(22) Akagi, K. *J. Polym. Sci., Part A: Polym. Chem.* **2009**, *47*, 2463–2485.

(23) Williamson, A. W. *J. Chem. Soc.* **1852**, *4*, 229–239.

(24) (a) Sonogashira, K.; Tohda, Y.; Hagihara, N. *Tetrahedron Lett.* **1975**, *16*, 4467–4470. (b) Sonogashira, K. *J. Organomet. Chem.* **2002**, *653*, 46–49.

(25) (a) Miyaura, N.; Suzuki, A. *J. Chem. Soc., Chem. Commun.* **1979**, 866–867. (b) Miyaura, N.; Yamada, K.; Suzuki, A. *Tetrahedron Lett.* **1979**, *20*, 3437–40.

(26) Mitsunobu, O.; Yamada, M. *Bull. Chem. Soc. Jpn.* **1967**, *40*, 2380–2382.

(27) For LC conjugated polymers, such as di-LCPA, it is typical that endothermic and exothermic phase transition peaks are not clearly observed in DSC. Usually broad peaks are observed for LC conjugated polymers in DSC spectra; thus, POM was used to observe and determine the phase transitions of the di-LCPAs. Typical DSC curves of monomer 1 (**M1**) and polymer 1 (**PA1**) are shown in the Supporting Information, Figure S4.

(28) *Liquid Crystalline and Mesomorphic Polymers*; Shibaev, V. P., Lam, L., Eds.; Springer-Verlag: New York, 1994.

(29) Chien, J. C. W. Polymerization. In *Polyacetylene: Chemistry, Physics, and Material Science*; Academic Press: London, 1984; Chapter 2, pp 24−83.

(30) It is widely researched that tantalum-catalyzed polymerizations of disubstituted polyacetylenes give trans-rich polyacetylenes having a trans-transoid stereoisomer. Looking at the planar spatial structure of a double C═C bond, the strain of an individual double bond adopting cis-configuration is higher than that of the trans-double bond. This is due to the existence of a strong steric interaction between substituents located at the double bond in the cis-position compared to the trans-position. Thus the resultant trans main-chain structure is determined by the stronger tendency of disubstituted polyacetylene to minimize the strain of individual double bonds. Therefore, for disubstituted polyacetylene the trans-transoid configuration is most favored to minimize the steric hindrance of the substituents located between individual double bonds. One evidence that the present polymers adopt a trans-transoid structure is that no peak for cis- to trans- isomerization is present in the differential thermal analysis (DTA) of **PA1**, as seen in the Supporting Information (Figure S3).

(31) (a) Khotimsky, V. S.; Tchirkova, M. V.; Litvinova, E. G.; Rebrov, A. I.; Bordarenko, N. G. *J. Polym. Sci., Polym. Chem.* **2003**, *41*, 2133–2155. (b) Masuda, T. *J. Polym. Sci., Polym. Chem.* **2007**, *45*, 165–180.

(32) The lengths of the **PA7** side chains were calculated using Spartan modeling software. The side chain having the PCH50120P moiety has a length ($L_1$) computed as 36.0 Å, while the side chain with the PCH509 moiety has a length ($L_2$) of 26.4 Å. The monolayer type $S_m$ phase has a relationship of $d = L$. By contrast, a bilayer type $S_m$ phase has the interlayer distance twice that of the side chain length, $d = 2L$. Since the smectic interlayer distance ($d$) is comparable to the side chain ($L_1$), we can deduce that **PA7** exhibits a monolayer $S_m$B LC phase.

(33) Shibaev, V. P.; Plate, N. A. In *Advances in Polymer Science*; Gordon, M., Plate, N. M., Eds.; Springer-Verlag: New York, 1984; Vol. 60, p 173.

(34) The smectic B phase can be further distinguished as either the hexagonal smectic B phase ($S_m$B) or the crystalline smectic B phase (CrB). X-ray diffraction (XRD) can be used to distinguish between the two LC phases. Usually a sharp ring around 20° in $2\theta$ is observed for the hexagonal $S_m$B phase, which is indicative of the short-range interlayer distance between the smectic planes. This pattern is distinguishable from the crystalline CrB phase, in which many other peaks beyond 20° in $2\theta$ appear due to long-range order. In the present case, the sharp ring at 19.4° was observed at the XRD pattern of **PA7** (Figure 5b) while smaller peaks at the wide angle area, characteristic of the CrB phase, are not observed. Thus, with these XRD observations, **PA7** can be assigned as the hexagonal $S_m$B phase.

(35) *Liquid Crystals: Experimental Study of Physical Properties and Phase Transitions*; Kumar, S., Ed.; Cambridge University Press: Cambridge, 2001; pp 65−94.

(36) Cheng, Y. J.; Luh, T. Y. *Chem.—Eur. J.* **2004**, *10*, 5361–5368.